

Nr. 75  
3. November 2021

Preprint-Series: Department of Mathematics - Applied Mathematics

Photoacoustic inversion formulas using mixed data on  
finite time intervalls

F. Dreier, M. Haltmeier

 Applied Mathematics

---

Technikerstraße 13 - 6020 Innsbruck - Austria  
Tel.: +43 512 507 53803 Fax: +43 512 507 53898  
<https://applied-math.uibk.ac.at>

# PHOTOACOUSTIC INVERSION FORMULAS USING MIXED DATA ON FINITE TIME INTERVALS\*

Florian Dreier<sup>†</sup>      and      Markus Haltmeier<sup>†</sup>

## Abstract

We study the inverse source problem in photoacoustic tomography (PAT) for mixed data, which is a weighted linear combination of the acoustic pressure wave and its normal gradient on an observation surface. We consider the case where the data is only available on finite time intervals which accounts for real-world usage of PAT. Extending our previous work, we derive explicit formulas up to a smoothing integral on convex domains with a smooth boundary, yielding exact reconstruction for circular or elliptical domains. We also present numerical reconstruction of our new exact inversion formulas on finite time intervals and compare them with the reconstructions of our previous formulas for unlimited time wave measurements.

**Keywords.** Image reconstruction, wave equation, Abel integral equations, inversion formula, photoacoustic computed tomography.

**AMS subject classifications:** 35R30, 44A12, 35L05, 92C55.

## 1 Introduction

In recent decades, PAT has attracted considerable attention in biomedical optics. This imaging method aims at recovering the spatially varying absorption coefficient of an internal source by measuring the resulting acoustic waves detected outside of the object. Here, the absorption coefficient is with respect to external electromagnetic radiation. The acoustic measurements are acquired by so-called ultrasound detectors which lie on a surface surrounding the imaged object [23, 33, 34, 35, 36]. Such wave phenomena can be modelled by the  $n$ -dimensional wave equation

$$\begin{aligned} \partial_t^2 u(x, t) - \Delta u(x, t) &= 0 && \text{for } (x, t) \in \mathbb{R}^n \times (0, \infty), \\ u(x, 0) &= f(x) && \text{for } x \in \mathbb{R}^n, \\ (\partial_t u)(x, 0) &= g(x) && \text{for } x \in \mathbb{R}^n, \end{aligned} \tag{1.1}$$

---

\***Funding:** This work has been supported by the Austrian Science Fund (FWF), project P 30747-N32.

<sup>†</sup>Department of Mathematics, University of Innsbruck, Technikerstraße 13, A-6020 Innsbruck, Austria (Florian.Dreier@uibk.ac.at, Markus.Haltmeier@uibk.ac.at).

where  $f$  and  $g$  are the initial data and  $u: \mathbb{R}^n \times [0, \infty) \rightarrow \mathbb{R}$  the solution of the wave equation. In PAT it is assumed that  $g$  is the zero function and  $f$  has compact support in some open domain  $\Omega \subset \mathbb{R}^n$ . The function  $f$  describes the optical absorption coefficient at different positions whereby various types of the biological tissues can be detected, including brain tumor and skin melanoma (see, for example, [29, 32, 39]). In PAT, one is interested to determine this physical quantity by using the measured pressure waves on the observation surface  $\partial\Omega$ .

Most analytic reconstruction methods in PAT assume that the measurements correspond to the values of the solution  $u$  on  $\partial\Omega \times (0, \infty)$ , which is also known as the *Dirichlet trace* or *Dirichlet data* on  $\partial\Omega \times (0, \infty)$ . Depending on the measurement surface  $\partial\Omega$ , there exist for example explicit inversion formulas for the determination of  $f$  that require only knowledge of  $u|_{\partial\Omega \times (0, \infty)}$ . To name a couple of references, inversion formulas have been established for bounded smooth surfaces like spheres [12, 13, 20, 26, 28, 35], ellipses [3, 16, 17, 25, 30, 31] and also for unbounded smooth surfaces [2, 4, 5, 10, 18, 19, 24, 27, 28, 35] including planar, quadric hypersurfaces and cylindrical surfaces. In [6, 21, 22, 30], non-smooth and finite open measurement surfaces have been considered.

As pointed out in [11, 37], for example, the measured data from piezoelectric transducers is generally a combination of the acoustic field  $u$  and its normal gradient (normal derivative) of  $u$  on the observation surface  $\partial\Omega$ . Theoretical results on the problem of recovering  $f$  from the normal derivative of  $u$  (which is also referred to as the *Neumann trace* of  $u$ ) are rather rare in the literature. In [11, 14], an inversion formula for a smooth function  $g$  from the normal gradient of  $u$  in (1.1) with initial data  $(0, g)$  on spheres in 3D is presented. Recently, in [38] a series formula for spheres and in [7, 8] an exact inversion formula of back-projection type for ellipsoids in arbitrary dimensions has been derived.

Accounting for realistic measurements mentioned above, a more general measurement model, which includes both the Dirichlet and Neumann case, is given by the trace of

$$u_{a,b}(x, t) := au(x, t) + b\partial_\nu u(x, t), \quad (x, t) \in \partial\Omega \times (0, \infty)$$

on the measurement surface  $\partial\Omega \times (0, \infty)$  for some weights  $a, b \in \mathbb{R}$ . Throughout this article, we refer to these measurements as *mixed data* or *mixed trace*. Recovering the absorption coefficient from mixed data has previously been studied in [38] for spheres in arbitrary dimensions and in [7] for circles in two dimensions. Another mathematical model for piezoelectric sensors is proposed, for example, in [1].

## 1.1 Inversion from finite time intervals

In this paper, we study the case which finds practical application in real-world PAT. Specifically, we assume that the measurements are given only on a finite time interval  $(0, T)$ . Moreover, we consider mixed data as an output signal of the transducers. The problem of recovering the initial data  $(f, 0)$  from Dirichlet traces on a finite time interval has already been discussed in [12], where an inversion formula in dimension two has been

developed. More precisely, they used an inversion result for recovering the spherical means with centers lying on a circle in  $\mathbb{R}^2$  from its Dirichlet traces by solving an Abel-type integral equation. Hence, the values of solution of the wave equation for time points greater than the diameter of the circle can be recovered by knowing only the values for time points smaller than the diameter. We use a similar approach and derive relations between spherical means and Dirichlet traces as well as the *weighted spherical means* (which will be defined later) and Neumann traces in even dimensions. In case of odd dimensions, such additional considerations are not necessary, as we will later see.

## 1.2 Previous work

The subsequent calculations are based on our previous work in [7, 8], where we derived the reconstruction formulas

$$f(x) = \frac{1}{2^{\frac{n-2}{2}} \pi^{\frac{n}{2}}} (-1)^{\frac{n-2}{2}} \int_{\partial\Omega} \int_{\|x-y\|}^{\infty} \frac{(\partial_t t^{-1})^{\frac{n-2}{2}} \partial_\nu u(y, t)}{\sqrt{t^2 - \|x-y\|^2}} dt d\sigma(y) - \mathcal{K}_\Omega f(x), \quad (1.2)$$

and

$$f(x) = \frac{1}{(2\pi)^{\frac{n-1}{2}}} (-1)^{\frac{n-3}{2}} \int_{\partial\Omega} \left(\frac{1}{t} \partial_t\right)^{\frac{n-3}{2}} \left(\frac{1}{t} \partial_\nu u\right)(y, \|x-y\|) d\sigma(y) - \mathcal{K}_\Omega f(x), \quad (1.3)$$

over unbounded time intervals for Neumann traces, holding true in even and odd dimensions and for smooth functions  $f \in C_c^\infty(\Omega)$  with compact support in an open convex domains  $\Omega \subset \mathbb{R}^n$  with smooth boundary. For the Dirichlet data case, we make use of the explicit inversion formula (see [17])

$$f(x) = \frac{1}{2^{\frac{n-2}{2}} \pi^{\frac{n}{2}}} (-1)^{\frac{n-2}{2}} \nabla_x \cdot \int_{\partial\Omega} \nu(y) \int_{\|x-y\|}^{\infty} \frac{(\partial_t t^{-1})^{\frac{n-2}{2}} u(y, t)}{\sqrt{t^2 - \|x-y\|^2}} dt d\sigma(y) + \mathcal{K}_\Omega f(x), \quad (1.4)$$

being valid in even dimensions under the assumptions presented above. For the definition of the additional term  $\mathcal{K}_\Omega f$  the reader is referred to [8].

At this point, we remark that  $\mathcal{K}_\Omega f = 0$  for circular or elliptical domains [8, 17]. Therefore, in this article whenever an explicit formula for  $f$  depends on  $\mathcal{K}_\Omega f$ , the formula is exact for circular or elliptical domains.

## 1.3 Outline

The paper is organized as follows. First, we start with some notations being used throughout the article. Then, we derive solution formulas for the directional derivatives for the solution of wave equation in even dimensions. In section 2.3, we briefly discuss Abel integral equations and state the solution formula for the classical Abel integral equation followed by derivations of specific relations between the spherical mean transform and the solution of the wave equation as well as the normal derivative of the

spherical means and Neumann traces. As we will see, both the solution formula for directional derivatives and the derived results from Abel integral equations are leading to our main results in section 3, where we derive explicit inversion formulas for Neumann and Dirichlet traces on convex domains  $\Omega \subset \mathbb{R}^n$  with a smooth boundary as well as for mixed traces on circular domains over finite intervals  $(0, T)$ . Our restriction on the end time is that  $T$  has to be greater or equal than the diameter of the domain  $\Omega$ . Note that although only knowledge of the measurements on the time interval from zero to the diameter of  $\Omega$  are theoretically necessary, the numerical results in section 5 do not show the same numerical reconstructions for different end times. We will also compare the numerical results of our new inversion formulas with numerical results of formulas (1.2) and (1.4) for unbounded time intervals. Section 4 studies the inversion problem in odd dimensions. The article ends with a short conclusion and remaining lemmas which have been used in certain parts of the article.

## 2 Notation and preliminary results

### 2.1 Notation

Let  $\Omega \subset \mathbb{R}^n$  be an open set,  $x \in \Omega$  and  $f: \Omega \rightarrow \mathbb{R}$  differentiable at  $x$ . For a vector  $v \in \mathbb{R}^n$  we denote by  $D_v f(x)$  the directional derivative of  $f$  at  $x$  along the vector  $v$ , that is, for a sufficient small  $\varepsilon > 0$ , the derivative of the function

$$(-\varepsilon, \varepsilon) \rightarrow \mathbb{R}: t \mapsto f(x + tv)$$

at zero. If  $\Omega$  is bounded and  $x \in \partial\Omega$ , we also use the notation  $\partial_\nu f(x)$  for  $D_\nu f(x)$ , indicating the *normal derivative* of  $f$  at  $x$ , where  $\nu: \partial\Omega \rightarrow \mathbb{R}^n$  is the outward unit normal vector field of  $\Omega$ . For a function  $f: \mathbb{R}^n \times [0, \infty) \rightarrow \mathbb{R}$ , we also use the notation  $D_v f(x, t)$  and  $\partial_\nu f(x, t)$  to denote the directional derivative and normal derivative of  $f$  at  $(x, t) \in \mathbb{R}^n \times [0, \infty)$  with respect to the spatial variable. Note that the chain rule gives

$$D_v f(x, t) = \langle v, \nabla f(x, t) \rangle, \quad (x, t) \in \mathbb{R}^n \times [0, \infty), \quad (2.1)$$

where  $\nabla f(x, t)$  denotes the gradient of  $f$  in the spatial variable.

The spherical mean operator of an integrable function  $f: \mathbb{R}^n \rightarrow \mathbb{R}$  is defined as

$$\mathcal{M}f: \mathbb{R}^n \times [0, \infty) \rightarrow \mathbb{R}: (x, r) \mapsto \frac{1}{n\omega_n} \int_{\mathbb{S}^{n-1}} f(x + ry) d\sigma(y), \quad (2.2)$$

where  $\omega_n$  denotes the volume of  $n$ -dimensional unit ball and  $\mathbb{S}^{n-1}$  the  $n - 1$ -dimensional unit sphere in  $\mathbb{R}^n$ . Moreover, for brevity we write

$$\mathcal{M}_\nu f: \mathbb{R}^n \times [0, \infty) \rightarrow \mathbb{R}: (x, r) \mapsto \partial_\nu \mathcal{M}f(x, r),$$

denoting the normal derivative of  $\mathcal{M}f$  in the spatial variable or the *weighted spherical mean transform*.

For any function  $f: (a, c) \cup (c, b) \rightarrow \mathbb{R}$  with  $a < b$  and  $c \in (a, b)$ , which is integrable on  $(a, c - \varepsilon) \cup (c + \varepsilon, b)$  for all  $0 < \varepsilon < \min\{c - a, b - c\}$ , we write

$$\text{p. v.} \int_a^b f(x) dx := \lim_{\varepsilon \searrow 0} \left( \int_a^{c-\varepsilon} f(x) dx + \int_{c+\varepsilon}^b f(x) dx \right),$$

provided the above limit exists. This form of integral is known as the *Cauchy principle value* integral.

Lastly, we use  $\mathcal{P}$  to denote the operator which takes a function  $g \in C_c^\infty(\mathbb{B}^n)$  with compact support in the open unit ball in  $\mathbb{R}^n$  to the restriction of the solution of wave equation (1.1) with initial data  $(0, g)$  on  $\mathbb{S}^{n-1} \times [0, \infty)$ . Moreover, we use the symbol  $\mathcal{N}$  to indicate the operator which maps a function  $f \in C_c^\infty(\mathbb{B}^n)$  to the restriction of  $t^{n-2}\mathcal{M}f$  on  $\mathbb{S}^{n-1} \times [0, \infty)$ .

## 2.2 Solution formulas for the wave equation

As can be observed in [7, 8], the derivation of the inversion formulas for Neumann traces are largely based on the analytic expression of the solution of the wave equation. For example, in [9], there is presented the well-known solution formula

$$\begin{aligned} u(x, t) = & \frac{1}{\gamma_n \omega_n} \left[ \partial_t \left( \frac{1}{t} \partial_t \right)^{\frac{n-2}{2}} \left( \int_{\mathbb{B}_t^n(x)} \frac{f(y)}{\sqrt{t^2 - \|y - x\|^2}} dy \right) \right. \\ & \left. + \left( \frac{1}{t} \partial_t \right)^{\frac{n-2}{2}} \left( \int_{\mathbb{B}_t^n(x)} \frac{g(y)}{\sqrt{t^2 - \|y - x\|^2}} dy \right) \right]. \end{aligned} \quad (2.3)$$

for even dimensions  $n \geq 2$  and  $f, g \in C_c^\infty(\Omega)$ , where  $\mathbb{B}_t^n(x)$  is the open ball with radius  $t$  and center  $x$  in  $\mathbb{R}^n$  and  $\gamma_n := 2 \cdot 4 \cdots (n-2) \cdot n$ . Another representation formula is given by

$$\begin{aligned} u(x, t) = & \frac{n}{\gamma_n} \left[ \partial_t \left( \int_0^t \frac{r}{\sqrt{t^2 - r^2}} \left( \frac{1}{r} \partial_r \right)^{\frac{n-2}{2}} \left( r^{n-2} \mathcal{M}f(x, r) \right) dr \right) \right. \\ & \left. + \left( \int_0^t \frac{r}{\sqrt{t^2 - r^2}} \left( \frac{1}{r} \partial_r \right)^{\frac{n-2}{2}} \left( r^{n-2} \mathcal{M}g(x, r) \right) dr \right) \right], \end{aligned} \quad (2.4)$$

(see, for example, [8, Lemma 2.2]). Based on (2.4), we will derive an analytic expression for the directional derivative of the solution of the wave equation along a vector  $v \in \mathbb{R}^n$ , being used in section 3. Before that, we present another technical result for the operator  $\left( \frac{1}{r} \partial_r \right)^k r^{n-2} \circ \mathcal{M}$ , appearing in formula (2.4). Formula (2.3) will be used in section 3.3.

**Lemma 2.1.** *Let  $n \geq 2$  be an integer and  $f \in C_c^\infty(\Omega)$ . For every  $k \in \mathbb{N}$  and  $(x, r) \in \mathbb{R}^n \times (0, \infty)$ , we have*

$$\begin{aligned} & \left(\frac{1}{r}\partial_r\right)^k r^{n-2}\mathcal{M}f(x,r) \\ &= \sum_{l=0}^k c_{k,l}^{(n)} r^{n-(2k+1)+l} \frac{1}{\sigma(\mathbb{S}^{n-1})} \int_{\mathbb{S}^{n-1}} \sum_{i \in \{1, \dots, n\}^l} \partial^i f(x+ry) y^i d\sigma(y), \end{aligned}$$

where  $\partial^i := \partial_{i_1} \dots \partial_{i_k}$ ,  $y^i := y_{i_1} \dots y_{i_k}$  and the coefficients are recursively defined by  $c_{0,0}^{(n)} := 1$ ,  $c_{1,0}^{(n)} := n-2$ ,  $c_{1,1}^{(n)} := 1$ ,  $c_{\tilde{k},0}^{(n)} := c_{\tilde{k}-1,0}^{(n)}(n-2\tilde{k})$ ,  $c_{\tilde{k},\tilde{k}}^{(n)} := 1$  and  $c_{\tilde{k},l}^{(n)} := c_{\tilde{k}-1,l-1}^{(n)} + c_{\tilde{k}-1,l}^{(n)}(n-2\tilde{k}+l)$  for all  $\tilde{k} \in \{2, \dots, k\}$  and  $l \in \{1, \dots, \tilde{k}-1\}$ .

*Proof.* For the proof of this identity, we refer to [8, Lemma 3.4], where a proof of a similar identity can be found.  $\square$

Now, we will prove the desired analytic expression for directional derivative of the solution of the wave equation in even dimensions.

**Proposition 2.2.** *Let  $n \geq 2$  be even,  $v$  be a vector  $\mathbb{R}^n$ ,  $\Omega \subset \mathbb{R}^n$  an open domain and  $f, g \in C_c^\infty(\Omega)$ . Moreover, let  $u: \mathbb{R}^n \times [0, \infty) \rightarrow \mathbb{R}$  be the solution of (1.1).*

(i) *For all  $(x, t) \in \mathbb{R}^n \times (0, \infty)$  we have*

$$\begin{aligned} D_v u(x, t) &= \frac{n}{\gamma_n} \left[ \partial_t \left( \int_0^t \frac{r}{\sqrt{t^2 - r^2}} (r^{-1}\partial_r)^{\frac{n-2}{2}} (r^{n-2} D_v \mathcal{M}f(x, r)) dr \right) \right. \\ &\quad \left. + \left( \int_0^t \frac{r}{\sqrt{t^2 - r^2}} (r^{-1}\partial_r)^{\frac{n-2}{2}} (r^{n-2} D_v \mathcal{M}g(x, r)) dr \right) \right]. \end{aligned} \quad (2.5)$$

(ii) *For  $x \in \partial\Omega$  and  $k \in \mathbb{N}$  it holds*

$$\begin{aligned} & (\partial_t t^{-1})^k D_v u(x, t) \\ &= \frac{n}{\gamma_n} \left[ \left( \int_0^t \frac{r}{t\sqrt{t^2 - r^2}} \left( \partial_r r (r^{-1}\partial_r)^{\frac{n-2}{2}+k} r^{n-2} D_v \mathcal{M}f(x, r) \right) dr \right) \right. \\ &\quad \left. + (\partial_t t^{-1})^k \left( \int_0^t \frac{r}{\sqrt{t^2 - r^2}} (r^{-1}\partial_r)^{\frac{n-2}{2}} (r^{n-2} D_v \mathcal{M}g(x, r)) dr \right) \right]. \end{aligned} \quad (2.6)$$

*Proof.* (i) We start with the proof of the first identity. From Lemma 2.1 we see that  $\partial_i \left(\frac{1}{r}\partial_r\right)^{\frac{n-2}{2}} r^{n-2}\mathcal{M}f$  is a bounded function for  $1 \leq i \leq n$ . Therefore, interchanging the time derivative with the differential operator  $\partial_i$ , differentiating under the integral sign and interchanging  $\partial_i$  with  $\left(\frac{1}{r}\partial_r\right)^{\frac{n-2}{2}} r^{n-2}\mathcal{M}f$  yield

$$\begin{aligned} \partial_i u(x, t) &= \frac{n}{\gamma_n} \left[ \partial_t \left( \int_0^t \frac{r}{\sqrt{t^2 - r^2}} \left(\frac{1}{r}\partial_r\right)^{\frac{n-2}{2}} (r^{n-2} \partial_i \mathcal{M}f(x, r)) dr \right) \right. \\ &\quad \left. + \left( \int_0^t \frac{r}{\sqrt{t^2 - r^2}} \left(\frac{1}{r}\partial_r\right)^{\frac{n-2}{2}} (r^{n-2} \partial_i \mathcal{M}g(x, r)) dr \right) \right] \end{aligned}$$

for  $1 \leq i \leq n$ . Next, we apply the above relation and (2.1) on  $D_v u(x, t)$  to deduce

$$\begin{aligned} D_v u(x, t) &= \frac{n}{\gamma_n} \sum_{i=1}^n v_i \left[ \partial_t \left( \int_0^t \frac{r}{\sqrt{t^2 - r^2}} \left( \frac{1}{r} \partial_r \right)^{\frac{n-2}{2}} \left( r^{n-2} \partial_i \mathcal{M}f(x, r) \right) dr \right) \right. \\ &\quad \left. + \left( \int_0^t \frac{r}{\sqrt{t^2 - r^2}} \left( \frac{1}{r} \partial_r \right)^{\frac{n-2}{2}} \left( r^{n-2} \partial_i \mathcal{M}g(x, r) \right) dr \right) \right] \\ &= \frac{n}{\gamma_n} \left[ \partial_t \left( \int_0^t \frac{r}{\sqrt{t^2 - r^2}} \left( \frac{1}{r} \partial_r \right)^{\frac{n-2}{2}} \left( r^{n-2} \sum_{i=1}^n v_i \partial_i \mathcal{M}f(x, r) \right) dr \right) \right. \\ &\quad \left. + \left( \int_0^t \frac{r}{\sqrt{t^2 - r^2}} \left( \frac{1}{r} \partial_r \right)^{\frac{n-2}{2}} \left( r^{n-2} \sum_{i=1}^n v_i \partial_i \mathcal{M}g(x, r) \right) dr \right) \right] \end{aligned}$$

Finally, using (2.1) inside the integrals again shows the desired identity.

(ii) First, we consider the case  $k = 1$ . Applying integration by parts on the first term on the right-hand side in (2.5) yields the sum of two boundary terms plus the integral

$$\int_0^t \sqrt{t^2 - r^2} \partial_r \left( r^{-1} \partial_r \right)^{\frac{n-2}{2}} r^{n-2} D_v \mathcal{M}f(x, r) dr.$$

Since  $f$  has compact support in  $\Omega$  and  $y \in \partial\Omega$ , we see from the definition of the spherical mean operator that  $(r^{-1} \partial_r)^{\frac{n-2}{2}} r^{n-2} D_v \mathcal{M}f(x, r) = 0$  for sufficient small  $r > 0$ . Therefore, both boundary terms are equal to zero. Then, using Leibniz's integral rule implies

$$\left( t^{-1} \partial_t \right) D_v u(x, t) = \int_0^t \frac{r}{\sqrt{t^2 - r^2}} \left( r^{-1} \partial_r \right)^{\frac{n-2}{2}+1} r^{n-2} D_v \mathcal{M}f(x, r) dr.$$

Then, the second identity follows from the integral identity

$$\partial_t \int_0^t \frac{r h(r)}{\sqrt{t^2 - r^2}} dr = \frac{1}{t} \int_0^t \frac{r \partial_r r h(r)}{\sqrt{t^2 - r^2}} dr,$$

given in [12, Proposition 3.1]. The case  $k > 1$  can be shown by repeating the first argument  $k$ -times and an application of the above integral identity in the last step.  $\square$

*Remark 2.3.* Analogous to proof of equation (2.6) in Proposition 2.2, one can show that the formula

$$\begin{aligned} &\left( \partial_t t^{-1} \right)^k u(x, t) \\ &= \frac{n}{\gamma_n} \left[ \left( \int_0^t \frac{r}{t \sqrt{t^2 - r^2}} \left( \partial_r r \left( r^{-1} \partial_r \right)^{\frac{n-2}{2}+k} r^{n-2} \mathcal{M}f(x, r) \right) dr \right) \right. \\ &\quad \left. + \left( \partial_t t^{-1} \right)^k \left( \int_0^t \frac{r}{\sqrt{t^2 - r^2}} \left( r^{-1} \partial_r \right)^{\frac{n-2}{2}} \left( r^{n-2} \mathcal{M}g(x, r) \right) dr \right) \right]. \end{aligned} \quad (2.7)$$

for all  $(x, t) \in \mathbb{R}^n \times (0, \infty)$  holds.

### 2.3 Abel integral equations

Typical Abel integral equations have the form

$$\int_a^x \frac{u(r)}{(x-r)^{1-\alpha}} dr = f(x), \quad (2.8)$$

where  $-\infty \leq a < b \leq \infty$ ,  $a < x < b$  and  $\alpha \in (0, 1)$ . Here,  $f: (a, b) \rightarrow \mathbb{R}$  is a given function and  $u: (a, b) \rightarrow \mathbb{R}$  the function to be determined. In [15], it is mentioned that, for example, if  $f$  is absolute continuous, then (2.8) has a unique solution in  $L^1((a, b))$  and  $u$  is given by the formula

$$u(r) = \frac{1}{\Gamma(1-\alpha)\Gamma(\alpha)} \frac{d}{dr} \int_a^r \frac{f(x)}{(r-x)^\alpha} dx, \quad r \in (a, b). \quad (2.9)$$

As we observe from (2.4) and (2.5), the functions

$$\left(\frac{1}{r}\partial_r\right)^{\frac{n-2}{2}} r^{n-2} \mathcal{M}f(x, \cdot) \quad \text{and} \quad \left(\frac{1}{r}\partial_r\right)^{\frac{n-2}{2}} r^{n-2} D_v \mathcal{M}f(x, \cdot)$$

solve a similar integral equation as (2.8) in the time domain for a fixed point  $x \in \mathbb{R}^n$  and initial data  $(f, 0)$ . Under the additional assumption  $x \in \partial\Omega$ , we can transform (2.4) and (2.5) suitably to obtain the following relations.

**Proposition 2.4.** *Let  $n \geq 2$  be even,  $x \in \partial\Omega$ ,  $v \in \mathbb{R}^n$  and  $u: \mathbb{R}^n \times [0, \infty) \rightarrow \mathbb{R}$  the solution of (1.1) with initial  $(f, 0)$ . Then, we have for every radius  $r > 0$*

$$\left(\frac{1}{r}\partial_r\right)^{\frac{n-2}{2}} r^{n-2} \mathcal{M}f(x, r) = \frac{2\gamma_n}{\pi n} \int_0^r \frac{u(x, t)}{\sqrt{r^2 - t^2}} dt \quad (2.10)$$

and

$$\left(\frac{1}{r}\partial_r\right)^{\frac{n-2}{2}} r^{n-2} D_v \mathcal{M}f(x, r) = \frac{2\gamma_n}{\pi n} \int_0^r \frac{D_v u(x, t)}{\sqrt{r^2 - t^2}} dt. \quad (2.11)$$

*Proof.* We give a proof for (2.10). Relation (2.11) can be proved analogously.

First, we apply integration by parts and use the compactness of  $\mathcal{M}f(x, \cdot)$  to obtain for  $t > 0$

$$\begin{aligned} \int_0^t \frac{r}{\sqrt{t^2 - r^2}} \left(\frac{1}{r}\partial_r\right)^{\frac{n-2}{2}} \left(r^{n-2} \mathcal{M}f(x, r)\right) dr \\ = \int_0^t \sqrt{t^2 - r^2} \partial_r \left(\frac{1}{r}\partial_r\right)^{\frac{n-2}{2}} \left(r^{n-2} \mathcal{M}f(x, r)\right) dr. \end{aligned}$$

Hence, the Leibniz-rule for integrals and (2.4) imply

$$u(x, t) = \frac{n}{\gamma_n} \int_0^t \frac{t}{\sqrt{t^2 - r^2}} \partial_r \left(\frac{1}{r}\partial_r\right)^{\frac{n-2}{2}} \left(r^{n-2} \mathcal{M}f(x, r)\right) dr,$$

and therefore

$$\frac{1}{\sqrt{t}} \frac{\gamma_n}{n} u(x, \sqrt{t}) = \int_0^t \frac{1}{\sqrt{t-r'} 2\sqrt{r'}} \partial_r \left( \frac{1}{r} \partial_r \right)^{\frac{n-2}{2}} \left( r^{n-2} \mathcal{M}f(x, r) \right) \Big|_{r=\sqrt{r'}} dr'$$

by substituting  $r' = r^2$ . Now, we make use of formula (2.9) and the relation  $\Gamma(\frac{1}{2}) = \sqrt{\pi}$  to deduce for  $r > 0$

$$\frac{1}{2\sqrt{r'}} \partial_r \left( \frac{1}{r} \partial_r \right)^{\frac{n-2}{2}} \left( r^{n-2} \mathcal{M}f(x, r) \right) \Big|_{r=\sqrt{r'}} = \frac{\gamma_n}{\pi n} \left( \frac{d}{dr} \int_0^r \frac{u(x, \sqrt{t'})}{\sqrt{t'} \sqrt{r-t'}} dt' \right) \Big|_{r=\sqrt{r'}}.$$

Next, multiplying both sides with  $2\sqrt{r'}$  and applying the chain rule lead to

$$\partial_r \left( \frac{1}{r} \partial_r \right)^{\frac{n-2}{2}} r^{n-2} \mathcal{M}f(x, r) = \frac{\gamma_n}{\pi n} \frac{d}{dr} \int_0^{r^2} \frac{u(x, \sqrt{t'})}{\sqrt{t'} \sqrt{r^2-t'}} dt' = \frac{2\gamma_n}{\pi n} \frac{d}{dr} \int_0^r \frac{u(x, t)}{\sqrt{r^2-t^2}} dt,$$

where we substituted  $t$  with  $\sqrt{t'}$  in the last step. Finally, integrating both sides from zero to  $r$  and using the second statement in (2.1), we see that (2.10) holds.  $\square$

**Corollary 2.5.** *Under the assumptions of Proposition 2.4 we have*

$$\left( \frac{1}{r} \partial_r \right)^{n-2} r^{n-2} \mathcal{M}f(x, r) = \frac{2\gamma_n}{\pi n} \int_0^r \frac{(\partial_t t^{-1})^{\frac{n-2}{2}} u(x, t)}{\sqrt{r^2-t^2}} dt \quad (2.12)$$

and

$$\left( \frac{1}{r} \partial_r \right)^{n-2} r^{n-2} D_v \mathcal{M}f(x, r) = \frac{2\gamma_n}{\pi n} \int_0^r \frac{(\partial_t t^{-1})^{\frac{n-2}{2}} D_v u(x, t)}{\sqrt{r^2-t^2}} dt. \quad (2.13)$$

*Proof.* Again, we only show (2.12). Applying integration by parts on the right-hand side in (2.10) gives the sum of two boundary terms plus the integral

$$\frac{2\gamma_n}{\pi n} \int_0^r \sqrt{r^2-t^2} t^{-1} u(x, t) dt.$$

From solution formula (2.3) we see that  $t^{-1}u(x, t) = 0$  for sufficient small  $t > 0$  and therefore both boundary terms equal zero. Then, using the integral rule of Leibniz implies

$$\frac{1}{r} \partial_r \left( \frac{1}{r} \partial_r \right)^{\frac{n-2}{2}} r^{n-2} \mathcal{M}f(x, r) = \frac{2\gamma_n}{\pi n} \int_0^r \frac{(\partial_t t^{-1}) u(x, t)}{\sqrt{r^2-t^2}} dt.$$

The remaining claim follows by applying above arguments inductively.  $\square$

From now on, we assume that  $\Omega \subset \mathbb{R}^n$  is a convex domain with smooth boundary and  $T \geq \text{diam}(\Omega) := \sup \{\|x-y\| \mid x, y \in \Omega\}$ . Furthermore, for the rest of this article we denote by  $u: \mathbb{R}^n \times [0, \infty) \rightarrow \mathbb{R}$  the solution of the wave equation with initial data  $(f, 0)$ , for a given function  $f \in C_c^\infty(\Omega)$ .

### 3 Inversion on finite time intervals in even dimensions

In this section we present our main results for the even-dimensional case. The following theorems are based on the relations given in Proposition 2.2, 2.4 and the reconstruction formulas derived from them in Theorem 3.6 for inverting the weighted spherical mean transform. We will also see that explicit inversion formulas depend on a measurable kernel  $k_T: (0, T)^2 \rightarrow \mathbb{R}$ , which is independent of the spatial dimension  $n \geq 2$ .

#### 3.1 Inversion from Neumann data on finite time intervals

The first theorem presents an explicit inversion formula for determining the initial data of the wave equation from Neumann traces on the bounded manifold  $\partial\Omega \times (0, T)$ .

**Theorem 3.1.** *Let  $n \geq 2$  be an even number,  $f \in C_c^\infty(\Omega)$  be a smooth function with compact support in  $\Omega$  and  $k_T: (0, T)^2 \rightarrow \mathbb{R}$  be the kernel function defined by  $k_T(r_1, r_2) := \frac{2}{\pi\sqrt{|r_1^2 - r_2^2|}} \tilde{k}_T(r_1, r_2)$  for  $r_1 \neq r_2$ , where*

$$\tilde{k}_T(r_1, r_2) := \begin{cases} \frac{1}{2} \log \left( \frac{\sqrt{T^2 - r_2^2} - \sqrt{r_1^2 - r_2^2}}{\sqrt{T^2 - r_2^2} + \sqrt{r_1^2 - r_2^2}} \right), & r_1 > r_2, \\ \arctan \left( \frac{\sqrt{T^2 - r_1^2}}{\sqrt{r_2^2 - r_1^2}} \right), & r_1 < r_2, \end{cases}$$

and  $k_T(r_1, r_2) := 0$  for  $r_1 = r_2$ . Then, for every  $x \in \Omega$  we have

$$f(x) = \frac{2(-1)^{\frac{n-2}{2}}}{\omega_n \gamma_n} \int_{\partial\Omega} \int_0^T k_T(\|x - y\|, t) \left( \partial_{tt}^{-1} \right)^{\frac{n-2}{2}} \partial_\nu u(y, t) dt d\sigma(y) - \mathcal{K}_\Omega f(x), \quad (3.1)$$

where  $\omega_n$  denotes the volume of the  $n$ -dimensional unit ball and  $\gamma_n = 2 \cdot 4 \cdots (n-2) \cdot n$ .

The following two identities, which are explicit inversion formulas for the weighted spherical mean transform, are essential for the derivation of our reconstruction formula in Theorem 3.1.

**Theorem 3.2.** *For  $f \in C_c^\infty(\Omega)$  and  $x \in \Omega$ , the relations*

$$f(x) = \frac{2n(-1)^{\frac{n-1}{2}}}{\omega_n \gamma_n^2} \int_{\partial\Omega} \int_0^T \left( \partial_r r (r^{-1} \partial_r)^{n-2} r^{n-2} \mathcal{M}_\nu f(y, r) \right) \frac{\log \left( \frac{r + \|x - y\|}{|r - \|x - y\||} \right)}{2 \|x - y\|} dr d\sigma(y) - \mathcal{K}_\Omega f(x) \quad (3.2)$$

and

$$f(x) = \frac{2n(-1)^{\frac{n-2}{2}}}{\omega_n \gamma_n^2} \int_{\partial\Omega} \text{p. v.} \int_0^T \frac{r (r^{-1} \partial_r)^{n-2} r^{n-2} \mathcal{M}_\nu f(y, r)}{r^2 - \|x - y\|^2} dr d\sigma(y) - \mathcal{K}_\Omega f(x). \quad (3.3)$$

in even dimensions hold.

*Proof.* (i) Inserting relation (2.6) into to the reconstruction formula (1.2) lead to

$$f(x) = \frac{2n}{\gamma_n^2 \omega_n} (-1)^{\frac{n-2}{2}} \int_{\partial\Omega} \int_{\|x-y\|}^{\infty} \int_0^t \frac{r \partial_r r (r^{-1} \partial_r)^{n-2} r^{n-2} \mathcal{M}_\nu f(y, r)}{t \sqrt{t^2 - \|x-y\|^2} \sqrt{t^2 - r^2}} dr dt d\sigma(y) \quad (3.4)$$

$$- \mathcal{K}_\Omega f(x).$$

Since  $\|x-y\| < t$  and  $0 < r < \min\{T, t\}$  for  $(t, r) \in (0, \infty)^2$  if and only if  $0 < r < T$  and  $\max\{r, \|x-y\|\} < t$ , we obtain from Fubini's theorem

$$\begin{aligned} & \int_{\partial\Omega} \int_{\|x-y\|}^{\infty} \int_0^r \frac{|r \partial_r r (r^{-1} \partial_r)^{n-2} r^{n-2} \mathcal{M}_\nu f(y, r)|}{t \sqrt{t^2 - \|x-y\|^2} \sqrt{t^2 - r^2}} dr dt d\sigma(y) \\ &= \int_{\partial\Omega} \int_0^T \int_{\max\{\|x-y\|, r\}}^{\infty} \frac{|r \partial_r r (r^{-1} \partial_r)^{n-2} r^{n-2} \mathcal{M}_\nu f(y, r)|}{t \sqrt{t^2 - \|x-y\|^2} \sqrt{t^2 - r^2}} dt dr d\sigma(y) \\ &\leq C \int_{\partial\Omega} \int_0^T \int_{\max\{\|x-y\|, r\}}^{\infty} \frac{r}{t \sqrt{t^2 - \|x-y\|^2} \sqrt{t^2 - r^2}} dt dr d\sigma(y), \end{aligned}$$

where  $C := \sup \left\{ \left| \partial_r r (r^{-1} \partial_r)^{n-2} r^{n-2} \mathcal{M}_\nu f(y, r) \right| \mid (y, r) \in \partial\Omega \times (0, T) \right\}$ . Next, from Lemma A.1 we see that the above triple integral equals

$$\int_{\partial\Omega} \int_0^T \frac{1}{2 \|x-y\|} \log \left( \frac{r + \|x-y\|}{|r - \|x-y\||} \right) dr d\sigma(y).$$

Then, the monotonicity and rules of the logarithmic-function yield the boundedness of the above triple integral. Hence, the application of Fubini's theorem on the triple integral in (3.4) and the same calculations as before yield the first identity.

(ii) Treating the inner integral in the principle value sense, applying integration by parts and using that  $r (r^{-1} \partial_r)^{n-2} r^{n-2} \mathcal{M}_\nu f(y, \cdot)$  has compact support in  $(0, T)$  for  $y \in \partial\Omega$ , we observe that the inner integral on right-hand side in (3.2) is equal to the limit of

$$\begin{aligned} & \frac{r (r^{-1} \partial_r)^{n-2} r^{n-2} \mathcal{M}_\nu f(y, r)}{2c} \log \left( \frac{r+c}{\varepsilon} \right) \Big|_{r=c-\varepsilon} \\ & - \frac{r (r^{-1} \partial_r)^{n-2} r^{n-2} \mathcal{M}_\nu f(y, r)}{2c} \log \left( \frac{r+c}{\varepsilon} \right) \Big|_{r=c+\varepsilon} \\ & + \int_{(0, T) \setminus (c-\varepsilon, c+\varepsilon)} \frac{r (r^{-1} \partial_r)^{n-2} r^{n-2} \mathcal{M}_\nu f(y, r)}{r^2 - c^2} dr \end{aligned}$$

as  $\varepsilon \searrow 0$ , where we set for brevity  $c := \|x-y\|$ . Expanding the logarithm and applying the mean value theorem, the boundary term can be estimated by the sum of the two terms on right-hand side in

$$\begin{aligned} & \frac{1}{2c} \left| r \left( r^{-1} \partial_r \right)^{n-2} r^{n-2} \mathcal{M}_\nu f(y, r) \log(r+c) \right|_{r=c-\varepsilon} \\ & \quad - r \left( r^{-1} \partial_r \right)^{n-2} r^{n-2} \mathcal{M}_\nu f(y, r) \log(r+c) \Big|_{r=c+\varepsilon} \Big| \\ & \leq \frac{\varepsilon}{c} \sup_{r \in [c-\delta, c+\delta]} \left| \partial_r r \left( r^{-1} \partial_r \right)^{n-2} r^{n-2} \mathcal{M}_\nu f(y, r) \log(r+c) \right| \end{aligned}$$

and

$$\begin{aligned} & \frac{|\log(\varepsilon)|}{2c} \left| r \left( r^{-1} \partial_r \right)^{n-2} r^{n-2} \mathcal{M}_\nu f(y, r) \Big|_{r=c-\varepsilon} - r \left( r^{-1} \partial_r \right)^{n-2} r^{n-2} \mathcal{M}_\nu f(y, r) \Big|_{r=c+\varepsilon} \right| \\ & \leq \frac{|\varepsilon \log(\varepsilon)|}{c} \sup_{r \in [c-\delta, c+\delta]} \left| \partial_r r \left( r^{-1} \partial_r \right)^{n-2} r^{n-2} \mathcal{M}_\nu f(y, r) \right|, \end{aligned}$$

for sufficient small  $\delta > 0$ . Hence, letting  $\varepsilon \searrow 0$  shows that the limit of the boundary terms equals zero and therefore, Equation (3.3) holds.  $\square$

*Proof of Theorem 3.1.* For better readability, we divide the proof into several parts.

(i) Inserting relation (2.13) into the inner integral on the right-hand side in (3.3), using the definition of the integral in the principle value sense and applying Fubini's theorem lead to

$$\begin{aligned} & \frac{2\gamma_n}{\pi n} \lim_{\varepsilon \searrow 0} \int_{(0,T) \setminus (c-\varepsilon, c+\varepsilon)} \int_0^r \frac{r \left( \partial_t t^{-1} \right)^{\frac{n-2}{2}} \partial_\nu u(y, t)}{(r^2 - c^2) \sqrt{r^2 - t^2}} dt dr \\ & = \frac{2\gamma_n}{\pi n} \lim_{\varepsilon \searrow 0} \left( \int_0^{c-\varepsilon} \int_{I_{\varepsilon,t}} \frac{r \left( \partial_t t^{-1} \right)^{\frac{n-2}{2}} \partial_\nu u(y, t)}{(r^2 - c^2) \sqrt{r^2 - t^2}} dr dt \right. \\ & \quad + \int_{c-\varepsilon}^c \int_{c+\varepsilon}^T \frac{r \left( \partial_t t^{-1} \right)^{\frac{n-2}{2}} \partial_\nu u(y, t)}{(r^2 - c^2) \sqrt{r^2 - t^2}} dr dt \\ & \quad \left. + \int_c^T \int_{\max\{t, c+\varepsilon\}}^T \frac{r \left( \partial_t t^{-1} \right)^{\frac{n-2}{2}} \partial_\nu u(y, t)}{(r^2 - c^2) \sqrt{r^2 - t^2}} dr dt \right), \end{aligned}$$

where we used the abbreviations  $c := \|x - y\|$  and  $I_{\varepsilon,t} := (t, c - \varepsilon] \cup [c + \varepsilon, T)$  for fixed  $y \in \partial\Omega$ .

(ii) In the next step, we compute above inner integrals separately. The first inner integral can be split up into two integrals which, by Lemma A.2, can be evaluated to

$$f_{1,\varepsilon}(t) := \int_t^{c-\varepsilon} \frac{r}{(r^2 - c^2) \sqrt{r^2 - t^2}} dr = \frac{1}{2\sqrt{c^2 - t^2}} \log \left( \frac{\sqrt{c^2 - t^2} - \sqrt{(c-\varepsilon)^2 - t^2}}{\sqrt{c^2 - t^2} + \sqrt{(c-\varepsilon)^2 - t^2}} \right)$$

and

$$\begin{aligned} f_{2,\varepsilon}(t) &:= \int_{c+\varepsilon}^T \frac{r}{(r^2 - c^2)\sqrt{r^2 - t^2}} dr \\ &= \frac{1}{2\sqrt{c^2 - t^2}} \log \left( \frac{\sqrt{T^2 - t^2} - \sqrt{c^2 - t^2}}{\sqrt{T^2 - t^2} + \sqrt{c^2 - t^2}} \frac{\sqrt{(c + \varepsilon)^2 - t^2} + \sqrt{c^2 - t^2}}{\sqrt{(c + \varepsilon)^2 - t^2} - \sqrt{c^2 - t^2}} \right). \end{aligned}$$

Again by Lemma A.2, we see that the second inner integral also corresponds to

$$f_{3,\varepsilon}(t) := \frac{1}{2\sqrt{c^2 - t^2}} \log \left( \frac{\sqrt{T^2 - t^2} - \sqrt{c^2 - t^2}}{\sqrt{T^2 - t^2} + \sqrt{c^2 - t^2}} \frac{\sqrt{(c + \varepsilon)^2 - t^2} + \sqrt{c^2 - t^2}}{\sqrt{(c + \varepsilon)^2 - t^2} - \sqrt{c^2 - t^2}} \right),$$

whereas the last inner integral is equal to

$$f_{4,\varepsilon}(t) := \frac{1}{\sqrt{t^2 - c^2}} \left( \arctan \left( \frac{\sqrt{T^2 - c^2}}{\sqrt{t^2 - c^2}} \right) - \arctan \left( \frac{\sqrt{\max\{t, c + \varepsilon\}^2 - c^2}}{\sqrt{t^2 - c^2}} \right) \right).$$

(iii) In the last step of the proof, we show

$$\begin{aligned} \lim_{\varepsilon \searrow 0} \int_0^{c-\varepsilon} (f_{1,\varepsilon}(t) + f_{2,\varepsilon}(t)) (\partial_t t^{-1})^{\frac{n-2}{2}} \partial_\nu u(y, t) dt \\ = \int_0^c \log \left( \frac{\sqrt{T^2 - t^2} - \sqrt{c^2 - t^2}}{\sqrt{T^2 - t^2} + \sqrt{c^2 - t^2}} \right) \frac{(\partial_t t^{-1})^{\frac{n-2}{2}} \partial_\nu u(y, t)}{2\sqrt{c^2 - t^2}} dt, \\ \lim_{\varepsilon \searrow 0} \int_{c-\varepsilon}^c f_{3,\varepsilon}(t) (\partial_t t^{-1})^{\frac{n-2}{2}} \partial_\nu u(y, t) dt = 0 \end{aligned}$$

and

$$\begin{aligned} \lim_{\varepsilon \searrow 0} \int_c^T f_{4,\varepsilon}(t) (\partial_t t^{-1})^{\frac{n-2}{2}} \partial_\nu u(y, t) dt \\ = \int_c^T \arctan \left( \frac{\sqrt{T^2 - c^2}}{\sqrt{t^2 - c^2}} \right) \frac{(\partial_t t^{-1})^{\frac{n-2}{2}} \partial_\nu u(y, t)}{\sqrt{t^2 - c^2}} dt, \end{aligned}$$

which yield the claimed identity.

First, we write

$$\begin{aligned} f_{1,\varepsilon}(t) + f_{2,\varepsilon}(t) &= \frac{1}{2\sqrt{c^2 - t^2}} \left[ \log \left( \frac{\sqrt{T^2 - t^2} - \sqrt{c^2 - t^2}}{\sqrt{T^2 - t^2} + \sqrt{c^2 - t^2}} \right) \right. \\ &\quad \left. + \log \left( \frac{\sqrt{c^2 - t^2} - \sqrt{(c - \varepsilon)^2 - t^2}}{\sqrt{c^2 - t^2} + \sqrt{(c - \varepsilon)^2 - t^2}} \frac{\sqrt{(c + \varepsilon)^2 - t^2} + \sqrt{c^2 - t^2}}{\sqrt{(c + \varepsilon)^2 - t^2} - \sqrt{c^2 - t^2}} \right) \right]. \end{aligned}$$

Then, from Lemma A.3 we have

$$\begin{aligned} & \int_0^{c-\varepsilon} |f_{1,\varepsilon}(t) + f_{2,\varepsilon}(t)| \left| \left( \partial_t t^{-1} \right)^{\frac{n-2}{2}} \partial_\nu u(y, t) \right| dt \\ & \leq C_1 \int_0^c \frac{1}{2\sqrt{c^2 - t^2}} \left( \left| \log \left( \frac{\sqrt{T^2 - t^2} - \sqrt{c^2 - t^2}}{\sqrt{T^2 - t^2} + \sqrt{c^2 - t^2}} \right) \right| + \log(6 + \sqrt{2}) \right) dt, \end{aligned}$$

where  $C_1 := \sup \left\{ \left| \left( \partial_t t^{-1} \right)^{\frac{n-2}{2}} \partial_\nu u(y, t) \right| \mid t \in (0, \infty) \right\}$ . Hence, Lebesgue's theorem and the second statement in Lemma A.2 show the first identity.

The second limit can be seen to vanish by expanding the logarithm similarly and using the estimate

$$\begin{aligned} \int_{c-\varepsilon}^c |f_{3,\varepsilon}(t)| \left| \left( \partial_t t^{-1} \right)^{\frac{n-2}{2}} \partial_\nu u(y, t) \right| dt & \leq C_1 (C_2 + \log(6 + \sqrt{2})) \int_{c-\varepsilon}^c \frac{1}{2\sqrt{c^2 - t^2}} dt \\ & = \frac{C_1 (C_2 + \log(6 + \sqrt{2}))}{2c} \left( \frac{\pi}{2} - \arcsin \left( \frac{c - \varepsilon}{c} \right) \right), \end{aligned}$$

where  $C_2 := \sup \left\{ \left| \log \left( \frac{\sqrt{T^2 - t^2} - \sqrt{c^2 - t^2}}{\sqrt{T^2 - t^2} + \sqrt{c^2 - t^2}} \right) \right| \mid t \in [0, c] \right\}$ .

Finally, since arctan is bounded by  $\pi/2$ , applying Lebesgue's theorem again on the third limit yield the final statement.  $\square$

### 3.2 Inversion from Dirichlet data on finite time intervals

Now, we consider the inverse problem for Dirichlet data  $u$  on  $\partial\Omega \times (0, T)$ . By using the back-projection formula for the spherical mean operator in [17] and the ideas for Neumann traces from the previous subsection, we deduce the following result.

**Theorem 3.3.** *Let  $n \geq 2$  be an even number,  $f \in C_c^\infty(\Omega)$  be a smooth function with compact support in  $\Omega$  and  $k_T: (0, T)^2 \rightarrow \mathbb{R}$  be the kernel function as defined in Theorem 3.1. Then, for every  $x \in \Omega$  we have*

$$\begin{aligned} f(x) & = \frac{2(-1)^{\frac{n-2}{2}}}{\omega_n \gamma_n} \nabla_x \cdot \int_{\partial\Omega} \nu(y) \int_0^T k_T(\|x - y\|, t) \left( \partial_t t^{-1} \right)^{\frac{n-2}{2}} u(y, t) dt d\sigma(y) \\ & \quad + \mathcal{K}_\Omega f(x), \end{aligned} \quad (3.5)$$

where  $\omega_n$  denotes the volume of the  $n$ -dimensional unit ball and  $\gamma_n = 2 \cdot 4 \cdots (n-2) \cdot n$ .

*Proof.* In [17], it has been shown that

$$\begin{aligned} f(x) & = \frac{2n(-1)^{\frac{n-2}{2}}}{\omega_n \gamma_n^2} \nabla_x \cdot \int_{\partial\Omega} \nu(y) \text{p. v.} \int_0^{\text{diam}(\Omega)} \frac{r (r^{-1} \partial_r)^{n-2} r^{n-2} \mathcal{M}f(y, r)}{r^2 - \|x - y\|^2} dr d\sigma(y) \\ & \quad + \mathcal{K}_\Omega f(x). \end{aligned}$$

As we observe in the above formula, the inner integral has the same form to that one in (3.3). Thus, by inserting (2.12) into the above equation and using the same arguments as in the proof of Theorem 3.1, we immediately obtain (3.5).  $\square$

### 3.3 Inversion from mixed data on finite time intervals

In this section, we consider the problem of determining the initial data of the wave equation from measurements of the type  $u_{a,b}$  on the boundary of open balls  $\mathbb{B}_\rho^n(z)$  with radius  $\rho > 0$  and center  $z \in \mathbb{R}^n$ . The main result is as follows.

**Theorem 3.4.** *Let  $n \geq 2$  be an even number,  $\mathbb{B}_\rho^n(z) \subset \mathbb{R}^n$  the open ball with radius  $\rho > 0$  and center  $z \in \mathbb{R}^n$ ,  $f \in C_c^\infty(\mathbb{B}_\rho^n(z))$ ,  $a, b \in \mathbb{R}$  with  $b \neq 0$  and  $k_T: (0, T)^2 \rightarrow \mathbb{R}$  be the kernel function as defined in Theorem 3.1. Then, for every  $x \in \mathbb{B}_\rho^n(z)$  we have*

$$f(x) = \frac{2(-1)^{\frac{n-2}{2}}}{b\omega_n\gamma_n} \int_{\partial\mathbb{B}_\rho^n(z)} \int_{\|x-y\|}^{\infty} \frac{(\partial_t t^{-1})^{\frac{n-2}{2}} u_{a,b}(y, t)}{\sqrt{t^2 - \|x-y\|^2}} dt d\sigma(y) \quad (3.6)$$

and

$$f(x) = \frac{2(-1)^{\frac{n-2}{2}}}{b\omega_n\gamma_n} \int_{\partial\mathbb{B}_\rho^n(z)} \int_0^T k_T(\|x-y\|, t) (\partial_t t^{-1})^{\frac{n-2}{2}} u_{a,b}(y, t) dt d\sigma(y), \quad (3.7)$$

where  $\omega_n$  denotes the volume of the  $n$ -dimensional unit ball and  $\gamma_n = 2 \cdot 4 \cdots (n-2) \cdot n$ .

For the proof, we first derive formula (3.6), which requires measurements for every time point  $t > 0$ . Similarly as in the previous sections, we use then the derived exact inversion formula for unbounded time intervals to establish formula (3.7) that requires only measurements on the finite time interval  $(0, T)$ .

For the derivation of the first result, we make use of the inversion formulas in even dimensions (see [12])

$$f(x) = -2(\mathcal{P}^* t \partial_t^2 \mathcal{P} f)(x) \quad \text{and} \quad (3.8)$$

$$f(x) = -2(\mathcal{P}^* \partial_t t \partial_t \mathcal{P} f)(x) \quad (3.9)$$

for recovering  $f \in C_c^\infty(\mathbb{B}^n)$  from  $\mathcal{P}f$ . Here,  $\mathcal{P}^*$  denotes the formal adjoint operator of  $\mathcal{P}$ . We use an analytic expression of the adjoint  $\mathcal{P}^*$  for certain functions  $F: \mathbb{S}^{n-1} \times [0, \infty)$  from which we are able to deduce a range condition for the solution of wave equation with initial data  $(f, 0)$  presented in Lemma 3.5.

Note that in [12] there has been derived an representation of  $\mathcal{P}^*$  in the two-dimensional case for continuous functions  $F: \mathbb{S}^{n-1} \times [0, \infty)$  with sufficient small decay, i.e,  $F(y, t) = \mathcal{O}(t^{-\alpha})$  as  $t \rightarrow \infty$  for some  $\alpha > 0$ . For higher dimensions  $n > 2$ , we additionally assume that  $F$  is  $(n-2)/2$  times continuously differentiable on  $(0, \infty)$  in the second component,  $(t^{-1} \partial_t)^k t^{-1} F(y, t) = \mathcal{O}(t^{-\alpha})$  for  $0 \leq k \leq (n-4)/2$  and  $(\partial_t t^{-1})^{(n-2)/2} F(y, t) = \mathcal{O}(t^{-\alpha})$  as  $t \rightarrow \infty$ . Then, the adjoint of  $\mathcal{P}$  can be expressed as (see [14])

$$\mathcal{P}^* F(x) = \frac{(-1)^{\frac{n-2}{2}}}{\gamma_n \omega_n} \int_{\mathbb{S}^{n-1}} \int_{\|x-y\|}^{\infty} \frac{(\partial_t t^{-1})^{(n-2)/2} F(y, t)}{\sqrt{t^2 - \|x-y\|^2}} dt d\sigma(y), \quad x \in \mathbb{R}^n. \quad (3.10)$$

**Lemma 3.5.** *Let  $n \geq 2$  be an even number,  $\mathbb{B}_\rho^n(z) \subset \mathbb{R}^n$  the open ball with radius  $\rho > 0$  and center  $z \in \mathbb{R}^n$  and  $f \in C_c^\infty(\mathbb{B}_\rho^n(z))$ . Then, for every  $x \in \mathbb{B}_\rho^n(z)$  we have*

$$0 = \int_{\partial\mathbb{B}_\rho^n(z)} \int_{\|x-y\|}^{\infty} \frac{(\partial_t t^{-1})^{(n-2)/2} u(y, t)}{\sqrt{t^2 - \|x-y\|^2}} dt d\sigma(y). \quad (3.11)$$

*Proof.* In the following, we assume without loss of generality that  $z = 0$  and  $\rho = 1$ . The remaining statement follows from a translation and rescaling argument. Note that from the product rule we have  $\partial_t t \partial_t \mathcal{P} = \partial_t \mathcal{P} f + t \partial_t^2 \mathcal{P} f$  and therefore  $\partial_t \mathcal{P} f = \partial_t t \partial_t \mathcal{P} f - t \partial_t^2 \mathcal{P} f$ . Hence, subtracting (3.9) from (3.8) gives

$$0 = \mathcal{P}^* (\partial_t t \partial_t \mathcal{P} f - t \partial_t^2 \mathcal{P} f)(x) = (\mathcal{P}^* \partial_t \mathcal{P} f)(x).$$

Since  $\partial_t \mathcal{P} f$  fulfills the conditions for the analytic expression of  $\mathcal{P}^*$  in (3.10) (see, for example, (2.3) and [8, Lemma 3.4]), we deduce

$$0 = \int_{\mathbb{S}^{n-1}} \int_{\|x-y\|}^{\infty} \frac{(\partial_t t^{-1})^{(n-2)/2} \partial_t \mathcal{P} f(y, t)}{\sqrt{t^2 - \|x-y\|^2}} dt d\sigma(y).$$

From (1.1) we easily see that  $\partial_t \mathcal{P} f$  solves the wave equation with initial data  $(f, 0)$  and therefore, (3.11) is proved.  $\square$

*Proof of formula (3.6).* From (1.2) we have

$$f(x) = \frac{2(-1)^{\frac{n-2}{2}}}{b\omega_n \gamma_n} \int_{\partial\mathbb{B}_\rho^n(z)} \int_{\|x-y\|}^{\infty} \frac{(\partial_t t^{-1})^{\frac{n-2}{2}} b \partial_\nu u(y, t)}{\sqrt{t^2 - \|x-y\|^2}} dt d\sigma(y). \quad (3.12)$$

Furthermore, (3.11) implies

$$0 = \frac{2(-1)^{\frac{n-2}{2}}}{b\omega_n \gamma_n} \int_{\partial\mathbb{B}_\rho^n(z)} \int_{\|x-y\|}^{\infty} \frac{(\partial_t t^{-1})^{(n-2)/2} a u(y, t)}{\sqrt{t^2 - \|x-y\|^2}} dt d\sigma(y). \quad (3.13)$$

Hence, adding (3.12) and (3.13) leads to (3.12).  $\square$

As a consequence of Lemma (3.5), we obtain the following range conditions for the spherical mean operator in even dimensions.

**Lemma 3.6.** *Let  $f \in C_c^\infty(\mathbb{B}_\rho^n(z))$  be a smooth function with compact support in the open ball with radius  $\rho > 0$  and center  $z \in \mathbb{R}^n$ . Then, for every  $x \in \mathbb{B}_\rho^n(z)$  the range conditions*

$$0 = \int_{\partial\mathbb{B}_\rho^n(z)} \int_0^T \left( \partial_r r \left( r^{-1} \partial_r \right)^{n-2} r^{n-2} \mathcal{M}f(y, r) \right) \frac{\log \left( \frac{r + \|x-y\|}{|r - \|x-y\||} \right)}{2 \|x-y\|} dr d\sigma(y) \quad (3.14)$$

and

$$0 = \int_{\partial\mathbb{B}_\rho^n(z)} \text{p. v.} \int_0^T \frac{r \left( r^{-1} \partial_r \right)^{n-2} r^{n-2} \mathcal{M}f(y, r)}{r^2 - \|x-y\|^2} dr d\sigma(y) \quad (3.15)$$

for the spherical mean operator in even dimensions hold.

*Proof.* The statements follows from inserting formula (2.7) into (3.11) and analogous calculations as in the proof of Theorem 3.6.  $\square$

The last lemma in this section presents a range condition for the solution of the wave equation on the bounded manifold  $\partial\mathbb{B}_\rho^n(z) \times (0, T)$ , which is the key ingredient for the derivation of the second formula in Theorem 3.1.

**Lemma 3.7.** *Let  $n \geq 2$  be an even number,  $\mathbb{B}_\rho^n(z) \subset \mathbb{R}^n$  the open ball with radius  $\rho > 0$  and center  $z \in \mathbb{R}^n$  and  $f \in C_c^\infty(\mathbb{B}_\rho^n(z))$ . Then, for every  $x \in \mathbb{B}_\rho^n(z)$  we have*

$$0 = \int_{\partial\mathbb{B}_\rho^n(z)} \int_0^T k_T(\|x - y\|, t) \left( \partial_t t^{-1} \right)^{\frac{n-2}{2}} u(y, t) dt d\sigma(y). \quad (3.16)$$

*Proof.* Similarly to the proof of Theorem 3.3, we observe that inner integral in the range condition of (3.15) has the same form as in (3.3). Thus, by inserting the relation for the spherical mean transform (2.12) into (3.15) and using the same arguments as in the proof for Neumann traces, the right-hand side in (3.15) can be transformed to the double integral in (3.16).  $\square$

*Proof of formula (3.6).* Again, this follows from an addition of (3.1) and (3.16).  $\square$

## 4 Inversion on finite time intervals in odd dimensions

In the last section of this article, we present new results for recovering the initial data of the wave equation from measurements on finite time intervals in odd dimensions. In [8, 14, 17], for example, there have already been established explicit inversion formulas for the recovery of the initial data from Neumann and Dirichlet data on bounded time intervals for the odd-dimensional case. The derivations of such inversion formulas are based on the fact that the wave data on the boundary  $\partial\Omega$  equals zero for all time points greater than or equal to  $\text{diam}(\Omega)$ . This leads automatically to reconstruction formulas that require only wave data on  $\partial\Omega \times (0, \text{diam}(\Omega))$ . Therefore, we only investigate the inverse problem for recovering  $f$  from knowledge of mixed measurements. Again, we consider open balls  $\mathbb{B}_\rho^n(z)$  and their boundary as their measurement surface.

### 4.1 Inversion from mixed data on finite time intervals

The inverse problem of determining  $f$  from the wave data  $u_{a,b}$  on the boundary of open balls  $\mathbb{B}_\rho^n(z)$  between the time points zero and  $2\rho$  can be solved similarly to the even-dimensional case. The main statement reads as follows.

**Theorem 4.1.** *Let  $n \geq 3$  be an odd number,  $\mathbb{B}_\rho^n(z) \subset \mathbb{R}^n$  the open ball with radius  $\rho > 0$  and center  $z \in \mathbb{R}^n$ ,  $f \in C_c^\infty(\mathbb{B}_\rho^n(z))$  and  $a, b \in \mathbb{R}$  with  $b \neq 0$ . Then, for every  $x \in \mathbb{B}_\rho^n(z)$  we have*

$$f(x) = \frac{2(-1)^{\frac{n-3}{2}}}{bn\gamma_n\omega_n} \int_{\partial\mathbb{B}_\rho^n(z)} \left( t^{-2} \left( \partial_t t^{-1} \right)^{\frac{n-3}{2}} \right) u_{a,b}(y, \|x - y\|) d\sigma(y), \quad (4.1)$$

where  $\omega_n$  denotes the volume of the  $n$ -dimensional unit ball and  $\gamma_n = 1 \cdot 3 \cdots (n-2)$ .

The proof of Theorem 4.1 is based on the reconstruction formulas (see [14])

$$f(x) = c_n(\mathcal{N}^* \mathcal{D}^{(n-3)/2} t^{-1} \partial_t^2 t \mathcal{P} f)(x) \quad \text{and} \quad (4.2)$$

$$f(x) = c_n(\mathcal{N}^* t \mathcal{D}^{(n-3)/2} t^{-1} \partial_t t \partial_t \mathcal{P} f)(x) \quad \text{for } x \in \mathbb{B}^n, \quad (4.3)$$

which are valid in odd dimensions for recovering  $f \in C_c^\infty(\mathbb{B}^n)$  from  $\mathcal{P}f$ . Here,  $\mathcal{N}^*$  denotes the formal  $L^2$  adjoint of  $\mathcal{N}$ ,  $\mathcal{D} := \frac{1}{2t} \partial_t$  and  $c_n := \frac{(-1)^{(n-1)/2} \sqrt{\pi}}{\Gamma(n/2)}$ . In [13], there has been derived the explicit expression

$$\mathcal{N}^* F(x) = \frac{1}{n\omega_n} \int_{\mathbb{S}^{n-1}} \frac{F(y, \|x-y\|)}{\|x-y\|} d\sigma(y), \quad x \in \mathbb{R}^n, \quad (4.4)$$

provided that  $F: \mathbb{S}^{n-1} \times [0, \infty) \rightarrow \mathbb{R}$  is smooth and zero to infinite order in the time variable at  $t=0$ . Equation (4.4) and reconstruction formulas (4.2), (4.3) can be used to deduce the following range condition for the Dirichlet trace in odd dimensions which looks slightly different to that one in even dimensions.

**Lemma 4.2.** *Let  $n \geq 3$  be an odd number,  $\mathbb{B}_\rho^n(z) \subset \mathbb{R}^n$  the open ball with radius  $\rho > 0$  and center  $z \in \mathbb{R}^n$  and  $f \in C_c^\infty(\mathbb{B}_\rho^n(z))$ . Then, for every  $x \in \mathbb{B}_\rho^n(z)$  we have*

$$0 = \int_{\partial \mathbb{B}_\rho^n(z)} \frac{(1 - \|x-y\|)}{\|x-y\|} \left( (t^{-1} \partial_t)^{\frac{n-3}{2}} t^{-1} \right) u(y, \|x-y\|) d\sigma(y). \quad (4.5)$$

*Proof.* As in the even-dimensional case, we deduce from the product rule the relation  $\partial_t \mathcal{P} f = \partial_t^2 t \mathcal{P} f - \partial_t t \partial_t \mathcal{P} f$ . Then, subtracting (4.3) from (4.2) gives

$$\begin{aligned} 0 &= \mathcal{N}^*(\mathcal{D}^{(n-3)/2} t^{-1} \partial_t^2 t \mathcal{P} f - t \mathcal{D}^{(n-3)/2} \partial_t t \partial_t \mathcal{P} f)(x) \\ &= \mathcal{N}^*((1-t) \mathcal{D}^{(n-3)/2} t^{-1} \partial_t \mathcal{P} f)(x). \end{aligned}$$

Finally, using the explicit expression of (4.4) leads to

$$\begin{aligned} 0 &= \int_{\partial \mathbb{B}_\rho^n(z)} \frac{((1-t) \mathcal{D}^{(n-3)/2} t^{-1} \partial_t \mathcal{P} f)(y, \|x-y\|)}{\|x-y\|} d\sigma(y) \\ &= \int_{\partial \mathbb{B}_\rho^n(z)} \frac{(1 - \|x-y\|)}{\|x-y\|} \left( (t^{-1} \partial_t)^{\frac{n-3}{2}} t^{-1} \right) u(y, \|x-y\|) d\sigma(y), \end{aligned}$$

where we used again in the last step that  $\partial_t \mathcal{P} f$  is the unique solution of (1.1) with initial data  $(f, 0)$ .  $\square$

*Proof of Theorem 4.1.* In [8, Theorem 4.1], it has been shown

$$f(x) = \frac{2(-1)^{\frac{n-3}{2}}}{bn\gamma_n\omega_n} \int_{\partial \mathbb{B}_\rho^n(z)} \left( (t^{-1} \partial_t)^{\frac{n-3}{2}} t^{-1} \right) b \partial_\nu u(y, \|x-y\|) d\sigma(y).$$

Then, using (4.5) leads to

$$f(x) = \frac{2(-1)^{\frac{n-3}{2}}}{bn\gamma_n\omega_n} \int_{\partial \mathbb{B}_\rho^n(z)} \frac{\left( (t^{-1} \partial_t)^{(n-3)/2} t^{-1} \right) (au + b \partial_\nu u)(y, \|x-y\|)}{\|x-y\|} d\sigma(y),$$

which shows the final result.  $\square$

## 5 Numerical implementation and experiments

Following the theoretical results in sections 3 and 4, we now present numerical implementations in two dimensions of our new inversion formulas for wave measurements on finite time intervals and compare them with old formulas requiring unlimited time wave measurements. We will consider all three types of traces. For the sake of completeness, we briefly discuss how we discretized initial data and the corresponding wave measurements and elaborate how we numerically implemented our new inversion formulas. Throughout this section, we suppose that  $f$  has compact support in some ball  $\mathbb{B}_\rho^2(z) \subset \mathbb{R}^2$  with radius  $\rho > 0$  and center  $z \in \mathbb{R}^2$ .

### 5.1 Discretization of simulated data and numerical implementation of new inversion formulas

Let  $N$  denote the number samples in one direction,  $\Delta x = \frac{2\rho}{N-1}$  the step size and  $T \geq 2\rho$  the end time. Our goal is to determine discrete values of  $f$  on the uniform grid  $\{-\rho + i\Delta x \mid i \in \{0, \dots, N-1\}\}^2$  from discrete wave data  $\mathbf{m}_T[k, l]$  given on the points of the circle

$$y_k := z + \rho(\cos(\varphi_k), \sin(\varphi_k)), \quad k = 0, \dots, N_\varphi - 1$$

with  $N_\varphi := \lceil 2\rho\pi/\Delta x \rceil$ ,  $\varphi_k := k\Delta\varphi$  and  $\Delta\varphi := 2\rho\pi/N_\varphi$ , and time points

$$t_l = l\Delta t, \quad l = 0, \dots, N_t - 1,$$

where  $0 < \Delta t < T$  and  $N_t := \lceil T/\Delta t + 1 \rceil$ . The measurements  $\mathbf{m}_T[k, l]$  correspond either to the discrete values of a weighted Neumann trace  $\mathbf{n}[k, l]$  or a weighted Dirichlet trace  $\mathbf{d}_T[k, l]$  or a mixed trace  $\mathbf{mix}_T[k, l]$  at  $(y_k, t_l)$ . For the numerical simulation, we computed them by solving the wave equation with fast Fourier transform (FFT) on the whole grid and using interpolation to obtain the corresponding values on detector points  $y_k$ .

#### Implementation of formula for Neumann/mixed traces

First, we give details on the numerical realization of formula (3.1). Formula (3.7) can be implemented analogously. Now, given the discrete values of the Neumann trace  $\mathbf{n}_T[k, l] = \partial_\nu u(y_k, t_l)$ , we approximate (3.1) by

$$\begin{aligned} f(x_{i,j}) &= \frac{\rho}{\pi} \int_0^{2\pi} \int_0^T k_T(\|x_{i,j} - h(\varphi)\|, t) \partial_\nu u(h(\varphi), t) dt d\varphi \\ &\approx \frac{\rho\Delta\varphi}{\pi} \sum_{k=0}^{N_\varphi-1} \int_0^T k_T(\|x_{i,j} - y_k\|, t) \partial_\nu u(y_k, t) dt \end{aligned}$$

where  $h: (0, 2\pi) \rightarrow \mathbb{R}^2: \varphi \mapsto z + \rho(\cos(\varphi), \sin(\varphi))^T$  denotes a parametrization of  $\partial\mathbb{B}_\rho^2(z)$  and  $x_{i,j} = (-R + i\Delta x, -R + j\Delta x)^T$  a point on the grid for some  $0 \leq i, j \leq N-1$ . In

order to approximate the above inner integral, we first compute

$$\begin{aligned} \int_0^T k_T(t_l, t) \partial_\nu u(y_k, t) dt &\approx \sum_{m=1}^{N_t-1} \int_{t_{m-1}}^{t_m} k_T(t_l, t) \partial_\nu u(y_k, t) dt \\ &\approx \frac{2}{\pi} \sum_{m=1}^{N_t-1} \int_{t_{m-1}}^{t_m} \frac{t_m}{\sqrt{|t_m^2 - t_l^2|}} t_m^{-1} \tilde{k}_T(t_l, t_m) \partial_\nu u(y_k, t_m) dt \\ &= \frac{2}{\pi} \sum_{m=1}^{N_t-1} \left| \sqrt{|t_m^2 - t_l^2|} - \sqrt{|t_{m-1}^2 - t_l^2|} \right| t_m^{-1} \tilde{k}_T(t_l, t_m) \mathbf{n}_T[k, m] \end{aligned}$$

for  $0 \leq l \leq N_t - 2$ . Defining  $\mathbf{A}_T[l, m] := \left| \sqrt{|t_m^2 - t_l^2|} - \sqrt{|t_{m-1}^2 - t_l^2|} \right| t_m^{-1} \tilde{k}_T(t_l, t_m)$  and  $\mathbf{A}_T[l, 0] = 0$  for  $0 \leq l \leq N_t - 2$  and  $1 \leq m \leq N_t - 1$ , we finally use

$$\mathbf{F}_T(\mathbf{n}_T)[i, j] := \frac{2\rho\Delta\varphi}{\pi^2} \sum_{k=0}^{N_\varphi-1} \text{interpolate}((\mathbf{n}_T * \mathbf{A}'_T)[k, :], \|x_{i,j} - y_k\|)$$

as a discretization of formula (3.1), where the inner term expresses the interpolated value of  $\|x_{i,j} - y_k\|$  respectively the array  $(\mathbf{n}_T * \mathbf{A}'_T)[k, :]$  and time points from zero to  $N_t - 2$ . Here,  $\mathbf{A}'_T$  denotes the transpose of the matrix  $\mathbf{A}_T$ . Formula (1.2) for unbounded time intervals can be discretized in a similar way

$$\mathbf{F}_\infty(\mathbf{n}_T)[i, j] := \frac{\rho\Delta\varphi}{\pi} \sum_{k=0}^{N_\varphi-1} \text{interpolate}((\mathbf{n}_T * \mathbf{A}')[k, :], \|x_{i,j} - y_k\|)$$

by using the matrix  $\mathbf{A} \in \mathbb{R}^{N_t \times N_t}$  defined by

$$\mathbf{A}[i, j] := \begin{cases} \sqrt{t_j^2 - t_i^2} - \sqrt{t_{j-1}^2 - t_i^2}, & i < j, \\ 0, & \text{else,} \end{cases}$$

and cutting off the inner integral in (1.2) from  $T$  to infinity.

The corresponding discretized versions of formulas (3.6) and (3.7) are denoted by  $\mathbf{F}_\infty(\mathbf{mix}_T)$  and  $\mathbf{F}_T(\mathbf{mix}_T)$ .

### Implementation of formula for Dirichlet traces

From (3.5) we see that implementing the formula for Dirichlet data requires the numerical computation of the double integral for each component. Writting  $\nu(y_k) = (\cos(\varphi_k), \sin(\varphi_k))^T$  for  $0 \leq k \leq N_\varphi - 1$ , the double integrals can be numerically evaluated to

$$\mathbf{G}_T(\mathbf{d}_T)^1[i, j] := \sum_{k=0}^{N_\varphi-1} \cos(\varphi_k) \text{interpolate}((\mathbf{d}_T * \mathbf{A}'_T)[k, :], \|x_{i,j} - y_k\|) \quad \text{and}$$

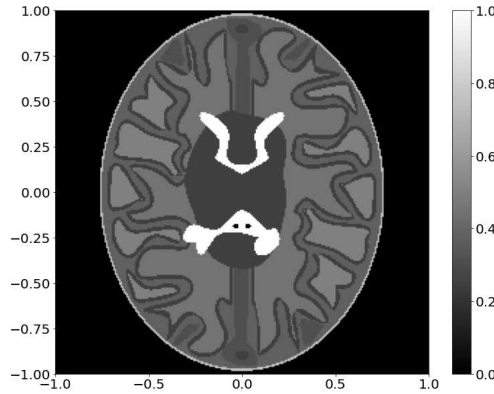


Figure 1: Initial data of our numerical experiment.

$$\mathbf{G}_T(\mathbf{d}_T)^2[i, j] := \sum_{k=0}^{N_\varphi-1} \sin(\varphi_k) \text{interpolate}((\mathbf{d}_T * \mathbf{A}'_T)[k, :], \|x_{i,j} - y_k\|),$$

resulting in the discretized formula

$$\mathbf{G}_T(\mathbf{d}_T)[i, j] := \frac{2\rho\Delta\varphi}{\pi^2} \left( CD^1(\mathbf{G}_T(\mathbf{d}_T)^1)[i, j] + CD^2(\mathbf{G}_T(\mathbf{d}_T)^2)[i, j] \right)$$

where  $CD^1$  and  $CD^2$  denote the central differences in  $x$  and  $y$  direction, respectively. The discretization  $\mathbf{G}_\infty(\mathbf{d}_T)$  of formula (1.4) can be approximated similarly by cutting off the inner integral from  $T$  to infinity, using  $\mathbf{A}$  instead of  $\mathbf{A}_T$  and changing the coefficient to  $\rho\Delta\varphi/\pi$ .

## 5.2 A numerical experiment

In the following, we perform our numerical computations on a  $[-1, 1] \times [-1, 1]$  grid with  $N := 257$  coordinate points. As initial data of the wave equation we use the same phantom being used in [7] (Figure 1), denoted by  $\mathbf{F} \in \mathbb{R}^{257 \times 257}$ . Note that the phantom has compact support in the open unit ball. We therefore assume that  $\mathbb{S}^1$  is the detection surface and  $\Delta t = 10^{-4}$  the time difference in which the simulated acoustic waves are measured. The end time is  $T = 2$  ( $=\text{diam}(\mathbb{B}^2)$ ), the shortest time for which our inversion formulas yield theoretically exact reconstruction. Figure 2 shows the different wave measurements of the head phantom with and without Gaussian noise added to the data. Here, 20% Gaussian noise added data means that normally distributed data with standard deviation 0.2 of the maximum was added to the original data. The two weights are set to  $a = 1$  and  $b = 1/10$ . The right column in Figure 3 shows the numerical approximations of our new inversion formulas over finite time intervals for Neumann and Dirichlet data ( $\mathbf{F}_T(\mathbf{n}_T)$  and  $\mathbf{G}_T(\mathbf{d}_T)$ ). We additionally plotted the numerical reconstructions of the filtered back-projection formulas requiring unlimited time measurements in the left column ( $\mathbf{F}_\infty(\mathbf{n}_T)$  and  $\mathbf{G}_\infty(\mathbf{d}_T)$ ). As we observe from our formulas for mixed data (3.6), (3.7) and the range conditions for Dirichlet traces in (3.11),

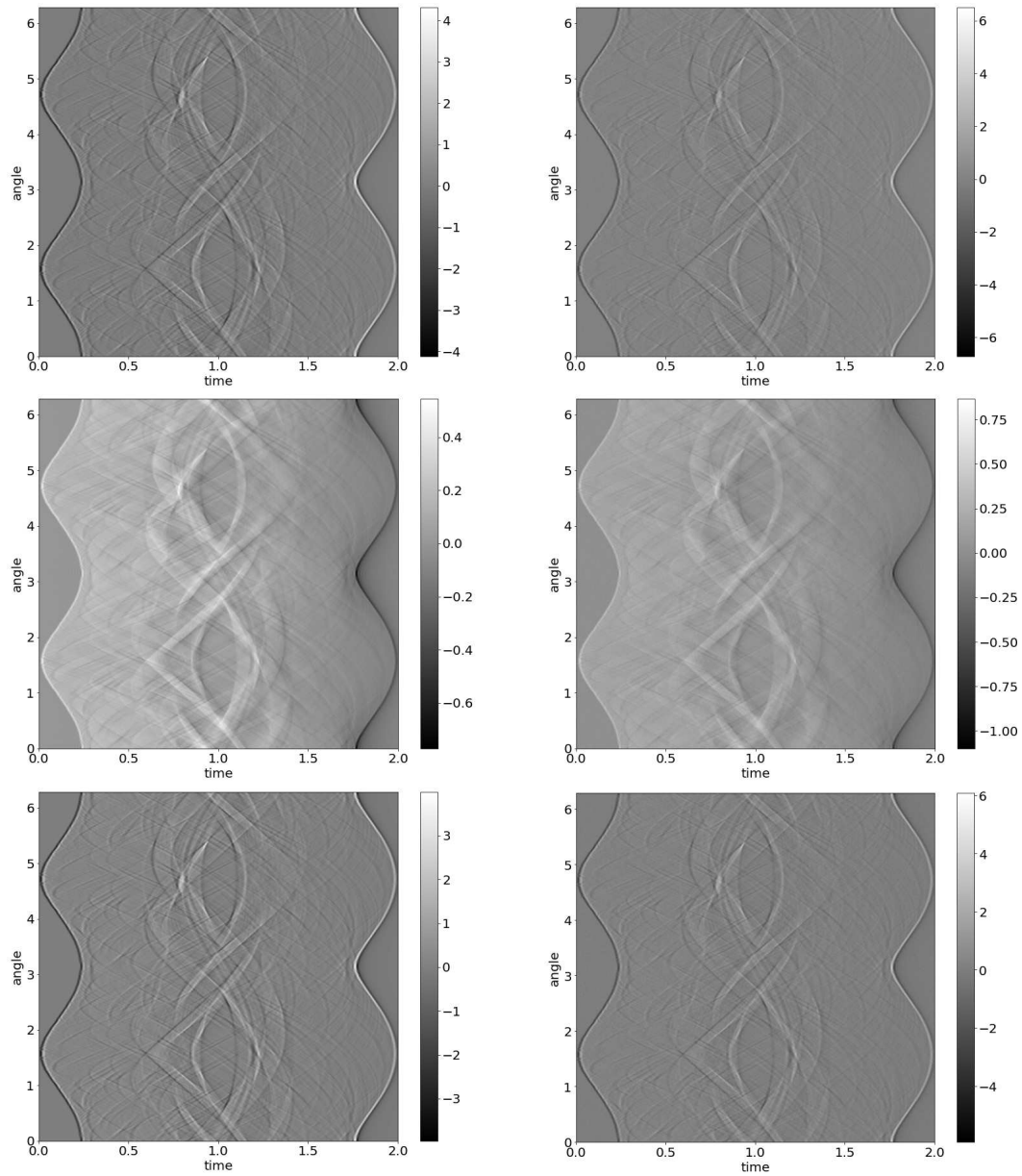


Figure 2: Simulated wave data. Top, left: Neumann data  $\mathbf{n}_T$ . Top, right: Neumann data  $\mathbf{n}_T$  with 20% Gaussian noise. Middle, left: Dirichlet data  $\mathbf{d}_T$ . Middle, right: Dirichlet data  $\mathbf{d}_T$  with 20% Gaussian noise. Below, left: mixed data  $\mathbf{mix}_T$ . Below, right: mixed data  $\mathbf{mix}_T$  with 20% Gaussian noise.

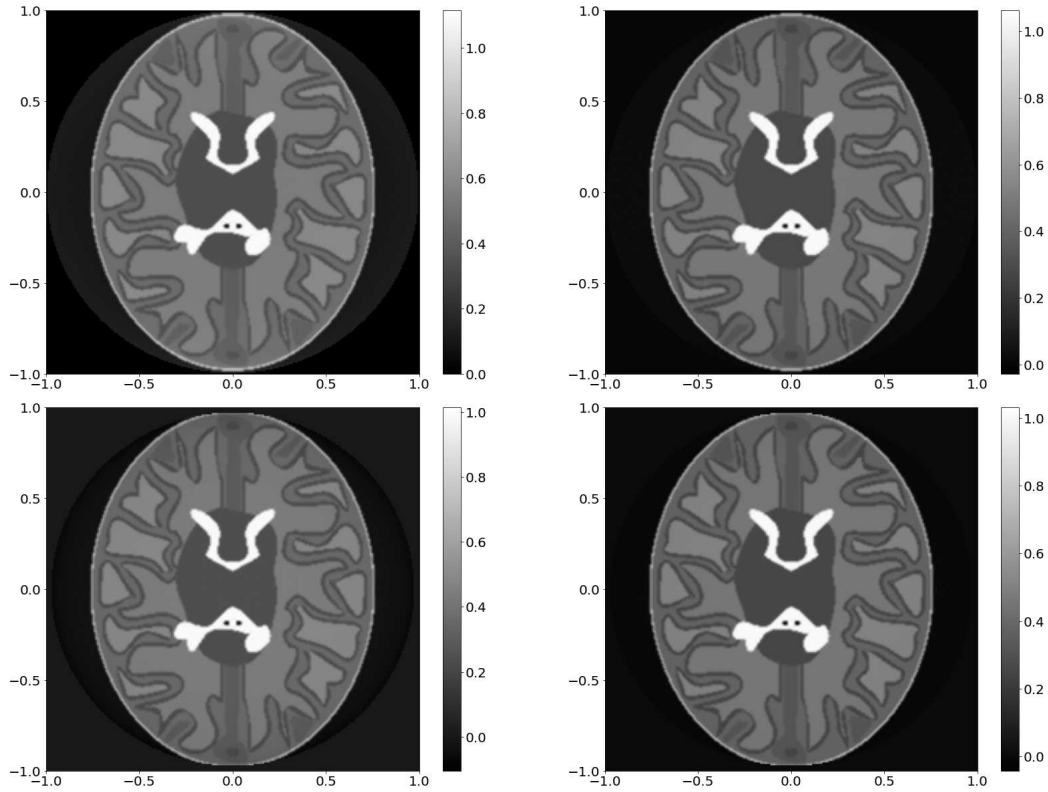


Figure 3: Reconstructions with exact data. Top, left:  $\mathbf{F}_\infty(\mathbf{n}_T)$ . Top, right:  $\mathbf{F}_T(\mathbf{n}_T)$ . Below, left:  $\mathbf{G}_\infty(\mathbf{d}_T)$ . Below, right:  $\mathbf{G}_T(\mathbf{d}_T)$ .

(3.16), an additional numerical error is made by using  $\mathbf{F}_T(\mathbf{mix}_T)$  and  $\mathbf{F}_T(\mathbf{mix}_T)$ . This error depends on the discrete approximations of the range conditions (with coefficients  $\rho/(\pi b)$  and  $2\rho/(\pi^2 b)$ ) corresponding to  $\mathbf{F}_\infty(\mathbf{d}_T)$  and  $\mathbf{F}_T(\mathbf{d}_T)$ , where  $\mathbf{n}_T$  is replaced by  $\mathbf{d}_T$  in the formulas  $\mathbf{F}_\infty(\mathbf{n}_T)$  and  $\mathbf{F}_T(\mathbf{n}_T)$ . In the first row in Figure 4, both errors without the weight  $b$  are presented. Due to the cut off of the improper integrals in (1.2) and (1.4) from  $T$  to infinity, we can detect a slight error inside the detection surface which doesn't belong to the phantom itself. The gray value outside of the phantom in the left reconstruction from Neumann data has approximately the constant value 0.12, whereas the right reconstruction with our new inversion formula hardly shows any error. A similar behaviour can be observed in the reconstructions from Dirichlet traces: The gray value on left image has here an approximate value of  $-0.05$  and the right image has values in the range of thousands.

A clear difference can be recognized in the error of the numerical implementations of the two different range conditions: The error of right reconstruction in the first row in Figure 4 is nearly seven times lower than the error in left image. This has a huge impact on the reconstructions  $\mathbf{F}_\infty(\mathbf{mix}_T)$  and  $\mathbf{F}_T(\mathbf{mix}_T)$  from mixed data as we will later see.

In order to study the stability of our inversion formulas, we also applied the dis-

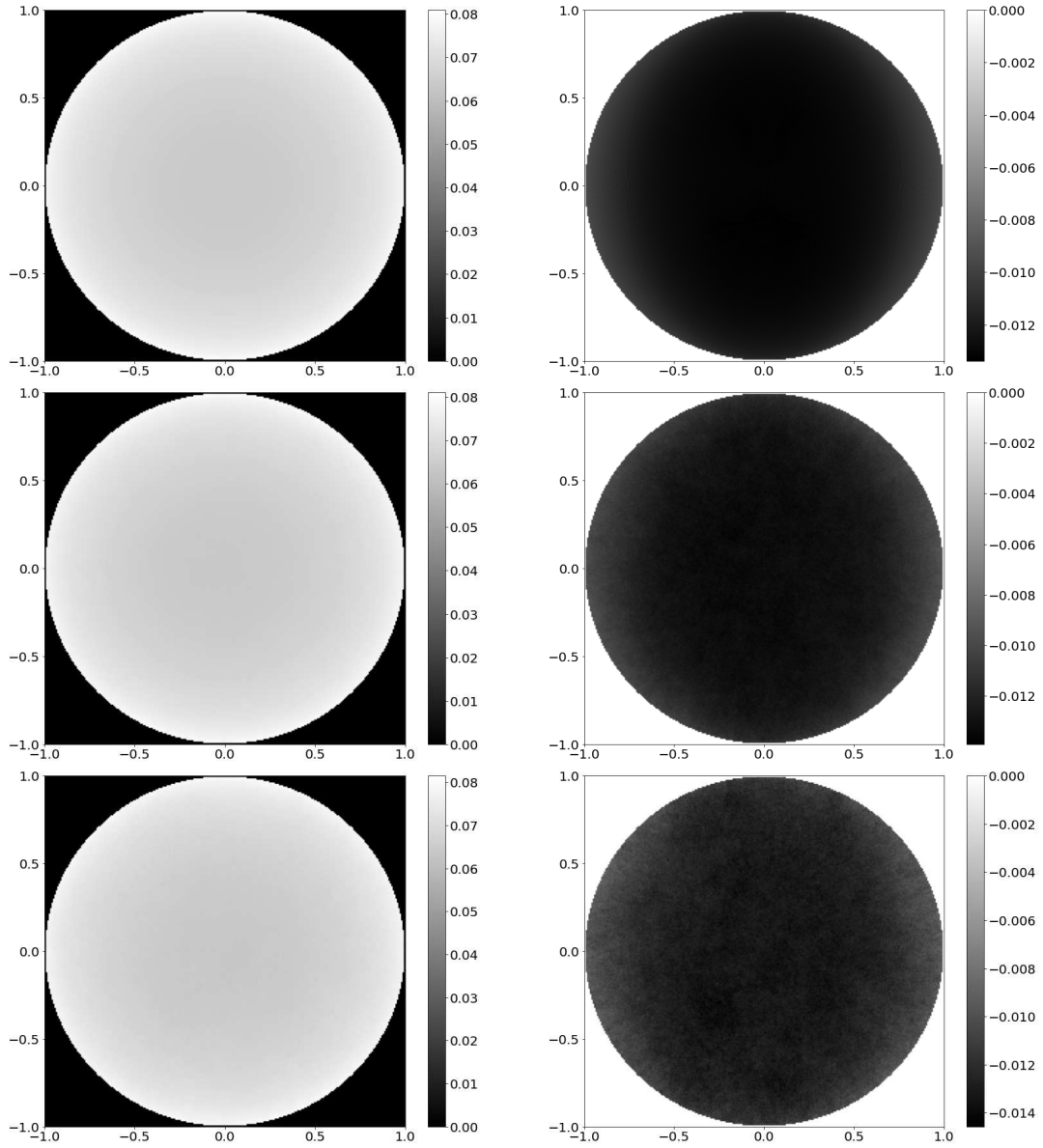


Figure 4: Discretization of the range conditions which should be equal to zero. Top:  $\mathbf{F}_\infty(\mathbf{d}_T)$  (left) and  $\mathbf{F}_T(\mathbf{d}_T)$  (right) with exact Dirichlet data. Middle:  $\mathbf{F}_\infty(\mathbf{d}_T)$  (left) and  $\mathbf{F}_T(\mathbf{d}_T)$  (right) with 20% Gaussian noise added Dirichlet data. Below:  $\mathbf{F}_\infty(\mathbf{d}_T)$  (left) and  $\mathbf{F}_T(\mathbf{d}_T)$  (right) with 40% Gaussian noise added Dirichlet data.

cretized formulas on noisy data. Figure 5 shows the obtained reconstructions using 20% Gaussian noise added data. Despite the added noise, we conclude that the disturbed

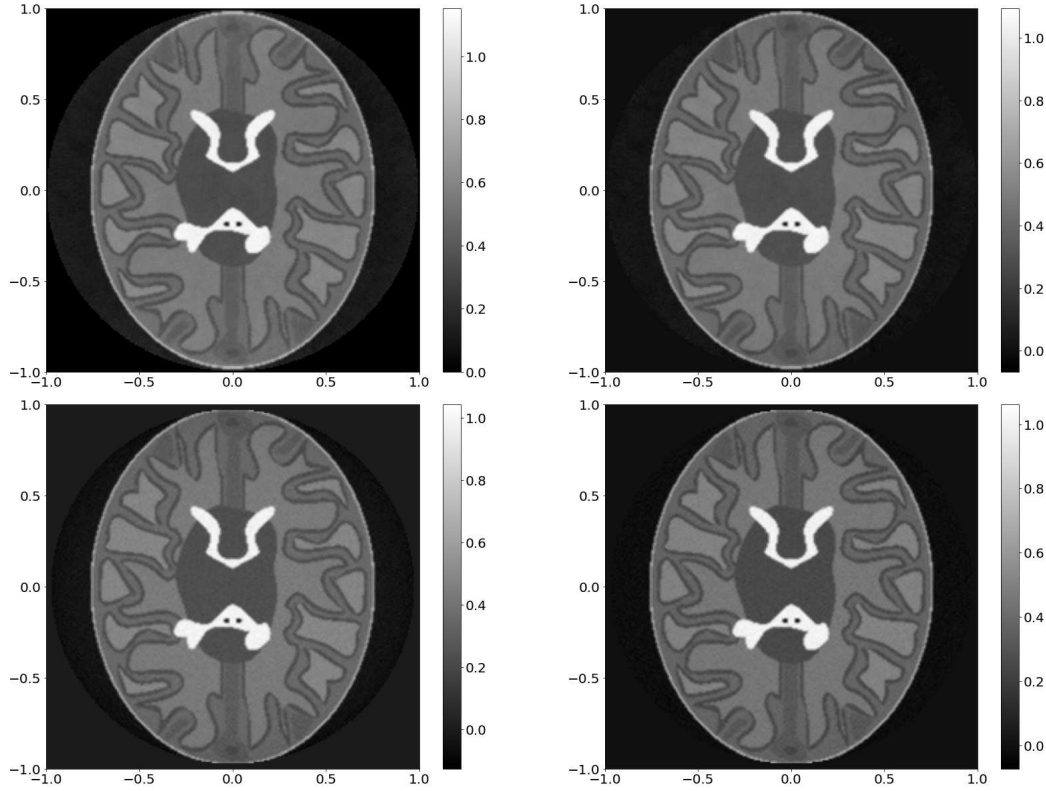


Figure 5: Reconstructions with 20% Gaussian noise added data. Top, left:  $\mathbf{F}_\infty(\mathbf{n}_T)$ . Top, right:  $\mathbf{F}_T(\mathbf{n}_T)$ . Below, left:  $\mathbf{G}_\infty(\mathbf{d}_T)$ . Below, right:  $\mathbf{G}_T(\mathbf{d}_T)$ .

data didn't strongly affect the recovery of our head phantom. The artefacts outside of reconstructions in the left column have become a bit stronger, whereas the right phantoms almost show any difference to the reconstructions with exact data.

In addition, we added more noise to the exact data and computed the numerical approximations of our inversion formulas with 40% Gaussian noise. The approximated phantoms are shown in Figure 6. Because of the higher noise rate in the data, we now obtain discrete values within the interval  $[-0.034, 0.477]$  and  $[-0.141, 0.351]$  outside of the phantom for  $\mathbf{F}_\infty(\mathbf{n}_T)$  and  $\mathbf{F}_T(\mathbf{n}_T)$ , respectively. The approximated formulas for Dirichlet traces yield the ranges  $[-0.169, 0.307]$  in  $\mathbf{G}_\infty(\mathbf{d}_T)$  and  $[-0.119, 0.329]$  in  $\mathbf{G}_T(\mathbf{d}_T)$ . Despite similar ranges, the discrete approximations of the exact formulas over finite time intervals show better results.

Lastly, we emphasize the big difference between the numerical reconstructions for mixed data. As already mentioned, the additional error of the discretization  $\mathbf{F}_\infty(\mathbf{n}_T)$  for Dirichlet data is many times higher than  $\mathbf{F}_T(\mathbf{n}_T)$ . This also holds for disturbed data (see Figure 4 middle, below). As demonstrated in Figure 7, the difference is clearly

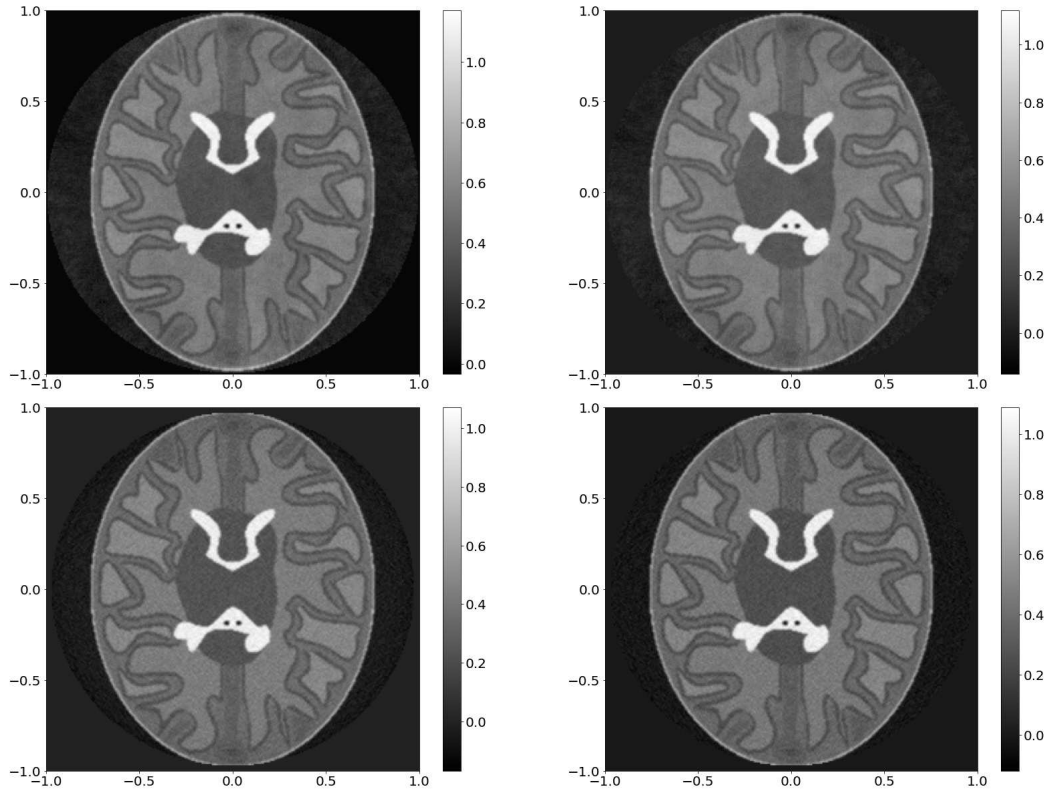


Figure 6: Reconstructions with 40% Gaussian noise added data. Top, left:  $\mathbf{F}_\infty(\mathbf{n}_T)$ . Top, right:  $\mathbf{F}_T(\mathbf{n}_T)$ . Below, left:  $\mathbf{G}_\infty(\mathbf{d}_T)$ . Below, right:  $\mathbf{G}_T(\mathbf{d}_T)$ .

visible for small weights such as  $b = 1/10$ .

### Varying the end time $T$

In the last section of article, we conclude our numerical results by calculating the single reconstructions for various end times  $T$  and compute their discrete  $L^2$ -error. The discrete  $L^2$ -error of  $\mathbf{F}_\infty(\mathbf{n}_T)$ , for example, is defined as

$$\left( \sum_{(i,j) \in \Omega_{\Delta x}} |\mathbf{F}_\infty(\mathbf{n}_T)[i,j] - \mathbf{F}[i,j]|^2 \Delta x^2 \right)^2,$$

where  $\Omega_{\Delta x} := \{(i,j) \in \{0, \dots, N-1\}^2 \mid x_{i,j} \in \mathbb{B}^2\}$ . The errors for the other reconstructions are defined in an analogous way. In Figure 8 the corresponding error plots of the single numerical reconstructions are shown. Note that the diagrams show the error of the reconstructions with 40% Gaussian noise. Moreover, due to the higher computation time for the simulation of the wave data, we selected a bigger time difference of  $\Delta t = 10^{-3}$ .

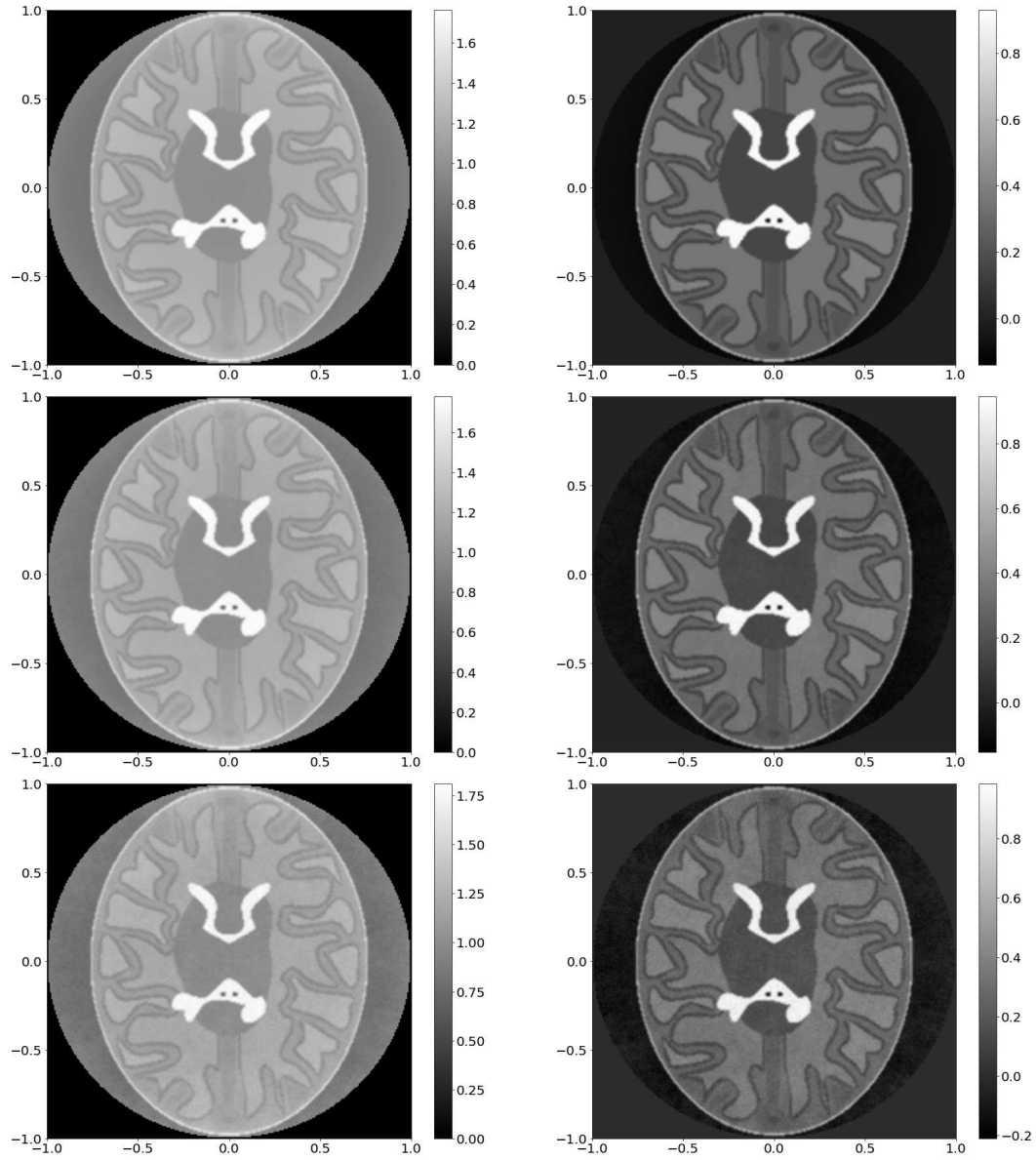


Figure 7: Reconstructions with mixed data. Top:  $\mathbf{F}_\infty(\mathbf{mix}_T)$  (left) and  $\mathbf{F}_T(\mathbf{mix}_T)$  (right) with exact data. Middle:  $\mathbf{F}_\infty(\mathbf{mix}_T)$  (left) and  $\mathbf{F}_T(\mathbf{mix}_T)$  (right) with 20% Gaussian noise. Below:  $\mathbf{F}_\infty(\mathbf{mix}_T)$  (left) and  $\mathbf{F}_T(\mathbf{mix}_T)$  (right) with 40% Gaussian noise.

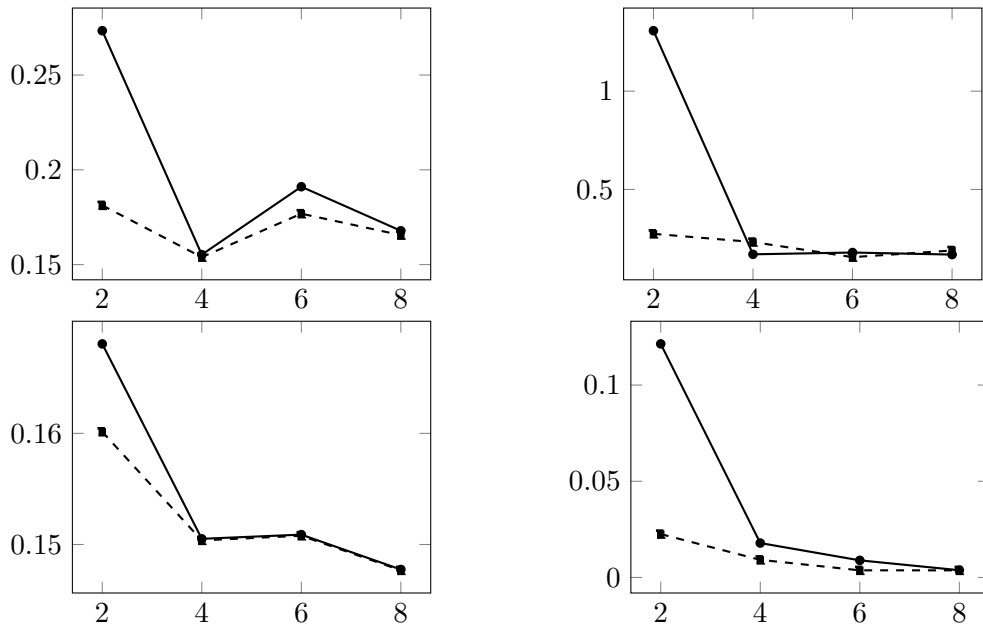


Figure 8:  $L^2$ -Error of the single reconstructions with 40% Gaussian noise for  $T = 2, 4, 6, 8$ : Top, left:  $\mathbf{F}_\infty(\mathbf{n}_T)$  (solid) and  $\mathbf{F}_T(\mathbf{n}_T)$  (dashed). Top, right:  $\mathbf{F}_\infty(\mathbf{mix}_T)$  (solid) and  $\mathbf{F}_T(\mathbf{mix}_T)$  (dashed). Below, left:  $\mathbf{G}_\infty(\mathbf{d}_T)$  (solid) and  $\mathbf{G}_T(\mathbf{d}_T)$  (dashed). Below, right:  $\mathbf{F}_\infty(\mathbf{d}_T)$  (solid) and  $\mathbf{F}_T(\mathbf{d}_T)$  (dashed).

We can clearly see that biggest difference between the reconstructions are for the shortest end time  $T = 2$ . With very few exceptions, the four discretized versions of the inversion formulas using finite time intervals have a smaller  $L^2$ -error for all end times as the ones using infinite time measurements. Moreover, we can see that the error values are tending to decrease as  $T$  is getting larger. We also observe that the larger the end time  $T$  is, the smaller the difference between the solid and dashed lines gets. Nevertheless, since in practice the acoustic waves are measured as shortly as possible due to external influences, the use of the new formulas offers a clear advantage for recovering the initial data of the wave equation.

## 6 Conclusion

In this article, we presented new reconstruction formulas for the inverse source problem in PAT requiring only measurements on finite time intervals. We provided inversion formulas of filtered back-projection type for the three types Dirichlet, Neumann and mixed data, whereas the formulas for the Dirichlet and Neumann data yields exact reconstruction for elliptical domains and the formula for mixed data on spheres in  $\mathbb{R}^n$ . In the even-dimensional case, we found a kernel function  $k_T : (0, T)^2 \rightarrow \mathbb{R}$  that can be used to recover the absorption coefficient independently of the spatial dimension  $n$  from

all three traces. We also observe that the formulas (1.2), (1.4) and (3.6) for unbounded time intervals can also be written in the form of a kernel function defined by

$$k_\infty: (0, \infty)^2 \rightarrow \mathbb{R}: (r_1, r_2) \mapsto \begin{cases} \frac{1}{\sqrt{r_2^2 - r_1^2}}, & r_2 > r_1, \\ 0, & \text{else.} \end{cases}$$

Then, it is not hard to see that this kernel satisfies the relation

$$k_\infty(r_1, r_2) = \lim_{T \rightarrow \infty} k_T(r_1, r_2), \quad (r_1, r_2) \in (0, \infty)^2,$$

meaning that sequence  $(k_T)_{T>0}$  converges pointwise by a zero extension on  $(0, \infty)^2$  to  $k_\infty$ . In the simulations we have seen that the numerical reconstructions of our new inversion formulas clearly show better results than the old formulas for unlimited time measurements, in particular the formula for mixed data. Therefore, the new photoacoustic inversion formulas provide a significant improvement to existing inversion formulas for unbounded time intervals, and thus for real-world applications in PAT.

## A Remaining lemmas

**Lemma A.1.** *Let  $a, b, c, d > 0$ ,  $a \neq b$  and  $\max\{a, b\} < c < d$ . Then, the following integral can be evaluated to*

$$\int_c^d \frac{1}{x\sqrt{x^2 - a^2}\sqrt{x^2 - b^2}} dx = F(d) - F(c), \quad (\text{A.1})$$

where  $F(x)$  is defined by the term

$$\frac{1}{2ab} \log \left( \left( \sqrt{\frac{x^2 - \max\{a, b\}^2}{x^2 - \min\{a, b\}^2}} + \frac{\max\{a, b\}}{\min\{a, b\}} \right) / \left( \frac{\max\{a, b\}}{\min\{a, b\}} - \sqrt{\frac{x^2 - \max\{a, b\}^2}{x^2 - \min\{a, b\}^2}} \right) \right),$$

for  $x > \max\{a, b\}$ , i.e.,  $F$  is an indefinite integral of the integrand in (A.1). Moreover,

$$\int_{\max\{a, b\}}^\infty \frac{1}{x\sqrt{x^2 - a^2}\sqrt{x^2 - b^2}} dx = \frac{1}{2ab} \log \left( \left( 1 + \frac{\max\{a, b\}}{\min\{a, b\}} \right) / \left( \frac{\max\{a, b\}}{\min\{a, b\}} - 1 \right) \right).$$

*Proof.* Assume, without loss of generality, that  $a < b$ . First, using the substitution  $x = \sqrt{u^2 + a^2}$  gives

$$\int_{u(c)}^{u(d)} \frac{1}{(u^2 + a^2)\sqrt{u^2 - (b^2 - a^2)}} du.$$

Next, we substitute  $u$  with  $\sqrt{b^2 - a^2} \sec(v)$  to obtain

$$\int_{v(u(c))}^{v(u(d))} \frac{\sec(v)}{(b^2 - a^2) \sec^2(v) + a^2} dv = \int_{v(u(c))}^{v(u(d))} \frac{\cos(v)}{b^2 - \sin^2(v)a^2} dv,$$

where we inserted the relation  $\sec(v) = \frac{1}{\cos(v)}$  and used the trigonometric identity  $\cos(v)^2 = 1 - \sin(v)^2$  afterwards. Thus, the final substitution  $w = \sin(v)$  leads to the standard integral

$$\frac{1}{a^2} \int_{w(v(u(c)))}^{w(v(u(d)))} \frac{1}{\frac{b^2}{a^2} - w^2} dw = \frac{1}{2ab} \left( \int_{w(v(u(c)))}^{w(v(u(d)))} \frac{1}{w + \frac{b}{a}} + \frac{1}{\frac{b}{a} - w} dw \right).$$

Finally, using the relation  $\sin(\operatorname{arcsec}(x)) = \frac{\sqrt{x^2-1}}{x}$  and inserting the upper and lower limit into the above integral yield the claimed identity.

The second statement is a consequence of the first integral identity, since  $F(\max\{a, b\}) = 0$  and the limit  $\lim_{d \rightarrow \infty} F(d)$  coincides with the right term in the second equality in Lemma A.1.  $\square$

**Lemma A.2.** *Let  $a, b, c, d \in \mathbb{R}$ ,  $a < b$ ,  $c \in [a, b]^c$ ,  $d \leq a$  and  $c \neq d$ . Then, we have the following identities:*

(i)

$$\begin{aligned} & \int_a^b \frac{x}{(x^2 - c^2)\sqrt{x^2 - d^2}} dx \\ &= \frac{1}{\sqrt{|c^2 - d^2|}} \begin{cases} \arctan\left(\frac{\sqrt{b^2 - c^2}}{\sqrt{d^2 - c^2}}\right) - \arctan\left(\frac{\sqrt{a^2 - c^2}}{\sqrt{d^2 - c^2}}\right), & c < d, \\ \frac{1}{2} \log\left(\left|\frac{\sqrt{c^2 - d^2} - \sqrt{b^2 - d^2}}{\sqrt{c^2 - d^2} + \sqrt{b^2 - d^2}} \frac{\sqrt{c^2 - d^2} + \sqrt{a^2 - d^2}}{\sqrt{c^2 - d^2} - \sqrt{a^2 - d^2}}\right|\right), & \text{else.} \end{cases} \end{aligned} \quad (\text{A.2})$$

(ii) For  $c > d$  we have

$$\lim_{\varepsilon \searrow 0} \frac{\sqrt{c^2 - d^2} - \sqrt{(c - \varepsilon)^2 - d^2}}{\sqrt{c^2 - d^2} + \sqrt{(c - \varepsilon)^2 - d^2}} \frac{\sqrt{(c + \varepsilon)^2 - d^2} + \sqrt{c^2 - d^2}}{\sqrt{(c + \varepsilon)^2 - d^2} - \sqrt{c^2 - d^2}} = 1. \quad (\text{A.3})$$

*Proof.* (i) We first substitute  $x$  with  $\sqrt{u^2 + d^2}$  to obtain the integral

$$\int_{u(a)}^{u(b)} \frac{1}{u^2 + d^2 - c^2} du.$$

If  $c < d$ , then using the substitution  $u = \sqrt{d^2 - c^2}v$  gives

$$\begin{aligned} & \frac{\sqrt{d^2 - c^2}}{d^2 - c^2} \int_{v(u(a))}^{v(u(b))} \frac{1}{1 + v^2} dv \\ &= \frac{1}{\sqrt{d^2 - c^2}} \left( \arctan\left(\frac{\sqrt{b^2 - c^2}}{\sqrt{d^2 - c^2}}\right) - \arctan\left(\frac{\sqrt{a^2 - c^2}}{\sqrt{d^2 - c^2}}\right) \right). \end{aligned}$$

If  $d > c$ , then

$$\int_{u(a)}^{u(b)} \frac{1}{u^2 - (c^2 - d^2)} du = \frac{1}{2\sqrt{c^2 - d^2}} \int_{u(a)}^{u(b)} \frac{1}{u - \sqrt{c^2 - d^2}} - \frac{1}{u + \sqrt{c^2 - d^2}} du.$$

Hence, the above integral equals

$$\frac{1}{2\sqrt{c^2 - d^2}} \log \left( \frac{\sqrt{c^2 - d^2} - \sqrt{b^2 - d^2} \sqrt{c^2 - d^2} + \sqrt{a^2 - d^2}}{\sqrt{c^2 - d^2} + \sqrt{b^2 - d^2} \sqrt{c^2 - d^2} - \sqrt{a^2 - d^2}} \right)$$

for  $b < c$  and

$$\frac{1}{2\sqrt{c^2 - d^2}} \log \left( \frac{\sqrt{b^2 - d^2} - \sqrt{c^2 - d^2} \sqrt{c^2 - d^2} + \sqrt{a^2 - d^2}}{\sqrt{c^2 - d^2} + \sqrt{b^2 - d^2} \sqrt{a^2 - d^2} - \sqrt{c^2 - d^2}} \right)$$

for  $b > c$ .

(ii) Applying L'Hospital's rule gives

$$\lim_{\varepsilon \searrow 0} \frac{\sqrt{c^2 - d^2} - \sqrt{(c - \varepsilon)^2 - d^2}}{\sqrt{(c + \varepsilon)^2 - d^2} - \sqrt{c^2 - d^2}} = \lim_{\varepsilon \searrow 0} \frac{c - \varepsilon}{\sqrt{(c - \varepsilon)^2 - d^2}} \frac{\sqrt{(c + \varepsilon)^2 - d^2}}{c + \varepsilon} = 1,$$

which implies the second statement in Lemma A.2.  $\square$

**Lemma A.3.** *Let  $c > 0$  be a positive number.*

(i) *Define*

$$g_\varepsilon: \mathbb{R} \rightarrow \mathbb{R}^+ : t \mapsto \begin{cases} \log \left( \frac{\sqrt{(c+\varepsilon)^2 - t^2} + \sqrt{c^2 - t^2}}{\sqrt{(c+\varepsilon)^2 - t^2} - \sqrt{c^2 - t^2}} \right), & t \in [c - \varepsilon, c], \\ 0, & \text{else.} \end{cases}$$

for  $\varepsilon > 0$ . Then,  $g_\varepsilon$  is a monotonically decreasing on  $[c - \varepsilon, c]$  and  $|g_\varepsilon| \leq \log(6 + \sqrt{2})$ .

(ii) *Let  $0 < \varepsilon < c$  and*

$$h_\varepsilon: \mathbb{R} \rightarrow \mathbb{R}^+ \\ t \mapsto \begin{cases} \log \left( \frac{\sqrt{c^2 - t^2} - \sqrt{(c-\varepsilon)^2 - t^2} \sqrt{(c+\varepsilon)^2 - t^2} + \sqrt{c^2 - t^2}}{\sqrt{c^2 - t^2} + \sqrt{(c-\varepsilon)^2 - t^2} \sqrt{(c+\varepsilon)^2 - t^2} - \sqrt{c^2 - t^2}} \right), & t \in [0, c - \varepsilon], \\ 0, & \text{else.} \end{cases}$$

Then,  $h_\varepsilon$  is a monotonically increasing on  $[0, c - \varepsilon]$  and  $|h_\varepsilon| \leq \log(6 + \sqrt{2})$ .

*Proof.* (i) By differentiating the inner fraction in  $g_\varepsilon$ , one easily verifies that the derivative is smaller than zero. Hence, from the monotonicity of the logarithmic function we imply that  $g_\varepsilon$  is a monotonically decreasing on  $[0, c - \varepsilon]$ . Furthermore, note that the inner fraction is greater or equal than one for  $t \leq c$  and

$$g_\varepsilon(c - \varepsilon) = \log \left( \frac{\sqrt{4c} + \sqrt{2c - \varepsilon}}{\sqrt{4c} - \sqrt{2c - \varepsilon}} \right).$$

Therefore, using that  $\varepsilon \mapsto \frac{\sqrt{4c} + \sqrt{2c - \varepsilon}}{\sqrt{4c} - \sqrt{2c - \varepsilon}}$  is decreasing for  $0 \leq \varepsilon \leq 2c$ , the first statement holds.

(ii) Differentiating the inner function in  $h_\varepsilon$  for  $t < c - \varepsilon$  with the product rule and a subsequent factorization lead to the expression

$$2t \frac{G(t)}{\sqrt{c^2 - x^2}} \left( \frac{1}{\sqrt{(c - \varepsilon)^2 - t^2}} - \frac{1}{\sqrt{(c + \varepsilon)^2 - t^2}} \right) > 0,$$

where  $G(t)$  denotes the inner function in  $h_\varepsilon$ . This implies the monotonicity of  $h_\varepsilon$  on  $[0, c - \varepsilon]$ . Then, the same arguments as in (i) show the remaining statement.  $\square$

## References

- [1] S. Acosta. Solvability for photoacoustic imaging with idealized piezoelectric sensors. *IEEE Trans. Ultrason., Ferroelectr., Freq. Control*, 67(11):2413–2422, 2020.
- [2] L.-E. Andersson. On the determination of a function from spherical averages. *SIAM J. Math. Anal.*, 19(1):214–232, 1988.
- [3] M. Ansorg, F. Filbir, W. R. Madych, and R. Seyfried. Summability kernels for circular and spherical mean data. *Inverse Problems*, 29(1):015002, 2012.
- [4] A. Beltukov. Inversion of the spherical mean transform with sources on a hyperplane. *arXiv preprint arXiv:0910.1380*, 2009.
- [5] A. L. Bukhgeim and V. B. Kardakov. Solution of the inverse problem for the equation of elastic waves by the method of spherical means. *Siberian Math. J.*, 19(4):528–535, 1978.
- [6] N. Do and L. A. Kunyansky. Theoretically exact photoacoustic reconstruction from spatially and temporally reduced data. *Inverse Problems*, 34(9):094004, 2018.
- [7] F. Dreier and M. Haltmeier. Explicit inversion formulas for the two-dimensional wave equation from Neumann traces. *SIAM J. Imaging Sci.*, 13(2):589–608, 2020.
- [8] F. Dreier and M. Haltmeier. Recovering the initial data of the wave equation from Neumann traces. *SIAM J. Math. Anal.*, 53(2):2427–2451, 2021.
- [9] L. C. Evans. *Partial Differential Equations*. American Mathematical Society, Second Edition, 2010.
- [10] J. A. Fawcett. Inversion of n-dimensional spherical averages. *SIAM J. Appl. Math.*, 45(2):336–341, 1985.
- [11] D. Finch. On a thermoacoustic transform. *Proc. 8th Int. Meeting on Fully 3D Image Reconstruction in Radiology and Nuclear Medicine*, pages 150–151, 2005.
- [12] D. Finch, M. Haltmeier, and Rakesh. Inversion of spherical means and the wave equation in even dimensions. *SIAM J. Appl. Math.*, 68(2):392–412, 2007.

- 
- [13] D. Finch, S. K. Patch, and Rakesh. Determining a function from its mean values over a family of spheres. *SIAM J. Math. Anal.*, 35(5):1213–1240, 2004.
- [14] D. Finch and Rakesh. The spherical mean value operator with centers on a sphere. *Inverse Problems*, 23(6):S37, 2007.
- [15] R. Gorenflo and S. Vessella. *Abel integral equations*, volume 1461. Springer, 1991.
- [16] M. Haltmeier. Inversion of circular means and the wave equation on convex planar domains. *Comput. Math. Appl.*, 65(7):1025–1036, 2013.
- [17] M. Haltmeier. Universal inversion formulas for recovering a function from spherical means. *SIAM J. Math. Anal.*, 46(1):214–232, 2014.
- [18] M. Haltmeier and S. Pereverzyev Jr. Recovering a function from circular means or wave data on the boundary of parabolic domains. *SIAM J. Imaging Sci.*, 8(1):592–610, 2015.
- [19] M. Haltmeier and S. Pereverzyev Jr. The universal back-projection formula for spherical means and the wave equation on certain quadric hypersurfaces. *J. Math. Anal. App*, 429(1):366–382, 2015.
- [20] L. A. Kunyansky. Explicit inversion formulae for the spherical mean Radon transform. *Inverse Problems*, 23(1):373, 2007.
- [21] L. A. Kunyansky. Reconstruction of a function from its spherical (circular) means with the centers lying on the surface of certain polygons and polyhedra. *Inverse Problems*, 27(2):025012, 2011.
- [22] L. A. Kunyansky. Inversion of the spherical means transform in corner-like domains by reduction to the classical Radon transform. *Inverse Problems*, 31(9):095001, 2015.
- [23] C. Li and L. V. Wang. Photoacoustic tomography and sensing in biomedicine. *Phys. Med. Biol.*, 54(19):R59–R97, 2009.
- [24] E. K. Narayanan and Rakesh. Spherical means with centers on a hyperplane in even dimensions. *Inverse Problems*, 26(3):035014, 2010.
- [25] F. Natterer. Photo-acoustic inversion in convex domains. *Inverse Probl. Imaging*, 6(2):1–6, 2012.
- [26] L. Nguyen. A family of inversion formulas in thermoacoustic tomography. *Inverse Probl. Imaging*, 3(4):649–675, 2009.
- [27] L. V. Nguyen. On a reconstruction formula for spherical radon transform: a microlocal analytic point of view. *Anal. Math. Phys.*, 4(3):199–220, 2014.

- 
- [28] S. J. Norton and M. Linzer. Ultrasonic reflectivity imaging in three dimensions: exact inverse scattering solutions for plane, cylindrical, and spherical apertures. *IEEE Trans. Biomed. Eng.*, (2):202–220, 1981.
- [29] J.-T. Oh, M.-L. Li, H. F. Zhang, K. Maslov, and L. V. Wang. Three-dimensional imaging of skin melanoma in vivo by dual-wavelength photoacoustic microscopy. *Journal of biomedical optics*, 11(3):034032, 2006.
- [30] V. P. Palamodov. Time reversal in photoacoustic tomography and levitation in a cavity. *Inverse Problems*, 30(12):125006, 2014.
- [31] Y. Salman. An inversion formula for the spherical mean transform with data on an ellipsoid in two and three dimensions. *J. Math. Anal. App*, 420(1):612–620, 2014.
- [32] J. Staley, P. Grogan, A. K. Samadi, H. Cui, M. S. Cohen, and X. Yang. Growth of melanoma brain tumors monitored by photoacoustic microscopy. *Journal of biomedical optics*, 15(4):040510, 2010.
- [33] L. V. Wang and S. Hu. Photoacoustic tomography: In vivo imaging from organelles to organs. *Science*, 335(6075):1458–1462, 2012.
- [34] X. Wang, Y. Pang, G. Ku, X. Xie, G. Stoica, and L. V. Wang. Noninvasive laser-induced photoacoustic tomography for structural and functional in vivo imaging of the brain. *Nat. Biotechnol.*, 21(7):803–806, 2003.
- [35] M. Xu and L. V. Wang. Universal back-projection algorithm for photoacoustic computed tomography. *Phys. Rev. E*, 71(1):016706, 2005.
- [36] M. Xu and L. V. Wang. Photoacoustic imaging in biomedicine. *Rev. Sci. Instrum.*, 77(4):041101, 2006.
- [37] Y. Xu and L. V. Wang. Time reversal and its application to tomography with diffracting sources. *Phys. Rev. Lett.*, 92(3):033902, 2004.
- [38] G. Zangerl, S. Moon, and M. Haltmeier. Photoacoustic tomography with direction dependent data: An exact series reconstruction approach. *Inverse Problems*, 35(11):114005, 2019.
- [39] H. F. Zhang, K. Maslov, G. Stoica, and L. V. Wang. Functional photoacoustic microscopy for high-resolution and noninvasive in vivo imaging. *Nat. Biotechnol.*, 24(7):848–851, 2006.